SUPPORTING INFORMATION

Programmable Multilayers of Nanometer-Sized Macrocycles on Solid Support and Stimuli-Controlled On-Surface Pseudorotaxane Formation

Johannes Poppenberg,[a] Sebastian Richter,[a] Christoph H.-H. Traulsen,[a] Erik Darlatt,[b] Bilge Baytekin,[c] Thomas Heinrich,[a] Peter M. Deutinger,[a] Katharina Huth,[a] Wolfgang E. S. Unger,*[b] Christoph A. Schalley*[a]

[a] Institut für Chemie und Biochemie, Freie Universität Berlin, Takustraße 3, 14195 Berlin, Germany

[b] BAM – Federal Institute for Materials Research and Testing, Unter den Eichen 44-46, 12203 Berlin, Germany

[c] Present address: Northwestern University, Dept, of Chemical and Biological Engineering, 2145 Sheridan Rd, Evanston, IL 60208, USA

Table of Contents:

General Methods

Synthetic reactions were conducted under a dry argon atmosphere. Dry solvents were purchased from ACROS Organics and used as received. Diethylether (Et_2O), hexane and ethylacetate were purchased from VWR and destilled prior to use by common laboratory methods. Ethanol (EtOH), dichloromethane (DCM), dimethylformamide (DMF), and acetonitrile (ACN) used for surface experiments were purchased from Carl Roth or VWR in HPLC grade and used as received. Silica gel 60M (0.04-0.063 mm, Machery-Nagel) was used for column chromatography. Gold substrates used for XPS and NEXAFS were prepared onto polished single-crystal Si(100) wafers which have been precoated with a 9 nm titanium adhesion layer and 30 nm gold. Semitransparent Au substrates (20 nm) used for transmission-UV/Vis-spectroscopy were prepared on borosilicate glass with a 1 nm titanium adhesion layer. For AFM experiments, epitaxially manufactured Au(111) substrates were used. All gold substrates were purchased from Georg Albert PVD and stored under argon prior to use. All surface experiments were performed in gamma-sterilized tubes (Orange Scientific).

Multilayers were prepared on **TDT**/**DT** (1 : 3) mixed, terpyridine-terminated self-assembled monolayers as template layer described before. As metal sources, iron(II) tetrafluoroborate hexahydrate, nickel(II) tetrafluoroborate hexahydrate and zinc tetrafluoroborate dihydrate were used, respectively. For metal deposition, the samples were immersed in a 1 mM solution of the metal salt in ethanol/water 1:1 for 30 min at r.t. Deposition of the macrocycle took place by immersing the samples in a 1 mM solution of **MC** in DMF for 24 h at r.t. For multilayer construction, both steps were alternatingly repeated until the desired number was reached. The squaraine dye was deposited by immersing the samples in a 1 mM solution of the dye in dichloromethane for 24 h at r.t. Removal of the dye was performed by immersing the sample in pure DMF or a 1 mM solution of tetrabutylammonium chloride in dichloromethane for 24 h at r.t. After each deposition step, the samples were immersed in the corresponding solvent (ethanol/water 1:1, DMF or dichloromethane) for another 10 min, dried vigorously in a stream of argon and stored under argon before characterization.

Instrumentation and Data Processing

NMR spectra were acquired on a Bruker ECX 400 (^{1}H at 400 MHz, ^{13}C at 101.8 MHz), a Joel Eclipse 500 (^{1}H: 500 MHz; ^{13}C: 125,8 MHz) and a Bruker 700 (^{1}H: 700 MHz; ^{13}C: 175 MHz) spectrometer at r.t. Exact masses were determined on an ESI-FTICR Ionspec QFT-7, Varian Inc. instrument. Transmission-UV/Vis-spectra were recorded on a Varian Cary 50 UV/Vis spectrophotometer. A spectrum of the underlying SAM was used as background and subtracted from all multilayer spectra.

AFM measurements were performed on a Multimode Nanosope V (Bruker) under atmospheric pressure at room temperature. As tips, NCL-W Point Probe and TAP150-G (Nanoworld) were used.

XPS measurements were carried out with an AXIS Ultra DLD electron spectrometer manufactured by Kratos Analytical, UK. XP spectra were recorded using monochromated Al K_α excitation at a pass energy of 40 eV for all detail spectra and 80 eV for the survey spectrum. The source-to-analyzer angle was 60°. Emission angles of 0° and 60° were used. The binding energy scales of XP spectra were corrected for charging using an electron binding energy of 83.96 eV for the Au $4f_{7/2}$ level of the gold substrate.[1] XP spectra were analyzed with Unifit 2013 fitting software (Unifit Scientific Software GmbH, Leipzig, Germany) and all peak fits were performed with a Lorentzian-Gaussian sum function peak shape model. The FWHM values in the N 1s and C 1s spectra were constrained to be equal for each component per spectrum. Peak fits and integrated peak areas were obtained after subtraction of Shirley backgrounds (Au $4f_{7/2}$, C 1s, F 1s Fe $2p_{3/2}$ and Ni $2p_{3/2}$). In case of N 1s this approach was not applicable because that low intensity peak is superimposed by the intense loss structure of the Au 4d photoemission doublet. A prerequisite for the application of a Shirley background is a higher count rate at the upper binding energy limit of the energy window used for background determination but in the given case (due to superposition of Au 4d) we have a lower count rate at the upper binding energy limit. As a workaround a linear background was used in this specific case. Of course, by doing this, the uncertainty of measurement will be increased but stayed at an acceptable level.

Layer thicknesses *d* were estimated utilizing XPS Au $4f_{7/2}$ signal intensity attenuation using the following equation:[2]

$$d = \lambda(\mathrm{KE}) \cdot cos\vartheta \cdot \ln\left(\frac{I_0}{I}\right)$$

Au $4f_{7/2}$ peak areas measured for covered surfaces (I) and from an Ar^+ ion-sputtered clean gold substrate (I_0) were used for calculation. A value for the inelastic mean free path of electrons λ(KE) = 3.8 nm was taken by averaging data obtained from relevant approaches.[3-7] The resulting *d* values were averaged for both applied emission angles $\vartheta = 0°$ and $\vartheta = 60°$.

NEXAFS measurements were carried out at the HESGM CRG dipole magnet beamline at the synchrotron radiation source BESSY II (Berlin, Germany). The spectra were acquired in the PEY (partial electron yield) mode using a channel plate detector with a retarding field of -150 V and incident angles of linearly polarized synchrotron light of 30° (electric field vector upright to surface plane) and 90° (electric field vector parallel to the surface plane).[8] The resolution E/ΔE of the monochromator at the carbonyl π^* resonance (hν = 287.4 eV) of CO was in the order of 2500. Raw spectra were divided by ring current and monochromator transmission function. The latter was obtained with a freshly sputtered Au sample.[8] Energy alignment of the energy scales was achieved by using an I_0 feature referenced to a C1s → π* resonance measured with a fresh surface of HOPG (highly ordered pyrolytic graphite, Advanced Ceramic Corp., Cleveland, USA) at 285.4 eV.[9]

Preparation and Characterization of New Compounds

The synthesis of diterpyridine tetralactam macrocycle **MC** (**Fig.** S1) was performed according to a modified literature-known procedure.[10] This reference describes also the syntheses of the precursors **1**, **2** and **5** as well as that of the monoterpyridine tetralactam macrocycle ***t*****BuMC**.

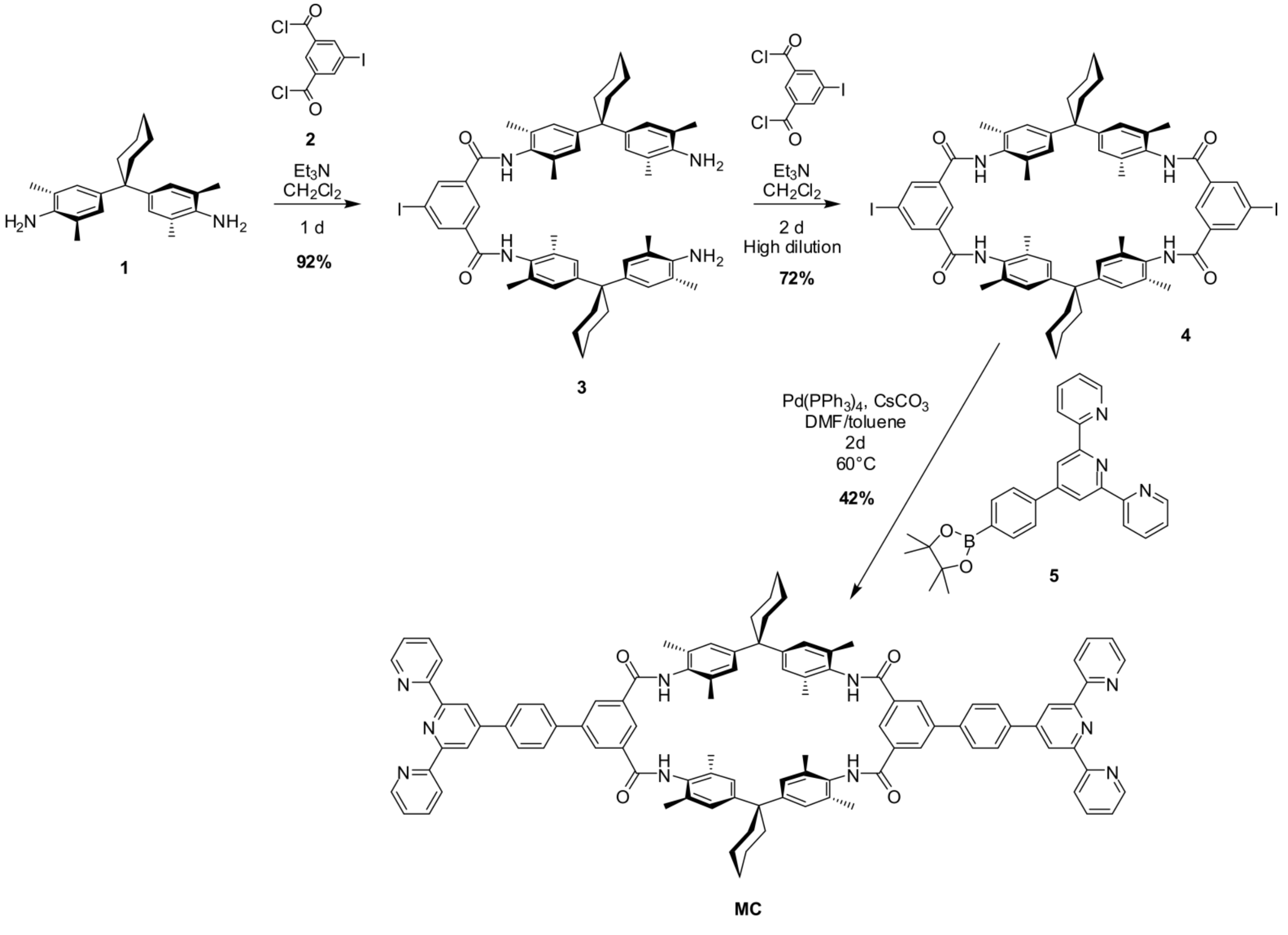

Fig. S1: Synthesis of diterpyridine macrocycle **MC**

N1,N3-Bis(4-(1-(4-amino-3,5-dimethylphenyl)cyclohexyl)-2,6-dimethylphenyl)-5-iodoisophthalamide (3). To a solution of 4,4'-(cyclohexane-1,1-diyl)bis(2,6-dimethylaniline) **1** (90.4 g, 280 mmol) in 1 l dichloromethane, 16 ml triethylamine were slowly added. Subsequently, 5-iodoisophthaloyl dichloride **2** (13.2 g, 40 mmol) dissolved in 2 l dichloromethane was added dropwise. The reaction was stirred at r.t. for 3 d. The solvent was removed under reduced pressure. Column chromatography on silica with dichloromethane/ethylacetate (1:1) as the eluent afforded 33.3 g (36.9 mmol) of pure product. Yield: 92%; ^{1}H NMR (400 MHz, DMSO-d_6) δ 9.87 (s, 2H, NH), 8.49 – 8.42 (m, 3H, isophth-H), 6.99 (s, 4H, Ar-H), 6.76 (s, 4H, Ar-H), 4.32 (s, 4H, NH_2), 2.23 – 2.15 (m, 8H, Cy-H), 2.12 (s, 12H, CH_3), 2.03 (s, 12H, CH_3), 1.55

– 1.34 (m, 12H, Cy-H); ^{13}C NMR (101 MHz, DMSO-*d*$_6$) δ 163.75, 148.72, 142.02, 138.95, 137.29, 135.62, 135.08, 132.33, 127.06, 126.73, 126.53, 120.86, 95.36, 44.60, 37.02, 26.49, 23.22, 19.03, 18.81; HR-MS (ESI, pos. mode): m/z: calcd. for $[C_{52}H_{62}N_4O_2I]^+$: 901.39119 ($[M+H]^+$); found: 901.38209.

11’,29’-Diiodo-5’,17’,23’,35’,38’,40’,43’,45’-octamethyldispiro[cyclohexane-1,2’-7’,15’,25’,33’-tetraazaheptacylo[32.2.2.$2^{3',6'}$.$2^{16',19'}$.$2^{21',24'}$.$1^{9',13'}$.$1^{27',31'}$]hexatetraconta-3’,5’,9’,11’,13’(44’),16’,18’,21’,23’,27’,29’,31’(39’),34’,36’,37’,40’,42’,45’-octadecaene-20’,1’’-cyclohexane]-8’,14’,26’,32’-tetraone (4). A solution of 3 (1.1 g, 1.22 mmol) and 2 ml triethylamine in 250 ml dichloromethane and a separately prepared solution of 2 (0.4 g, 1.22.mmol) in 250 ml dichloromethane were degased for 15 min. Subsequently, both solutions were added simultaneously with a peristaltic pump to 1.2 l of pure dichloromethane over a time period of 8 h. The reaction was stirred at r.t. for 24 h and the solvent then removed under reduced pressure. For purification, the crude product was refluxed in 200 ml of ethylacetate/methanol 1:1 to dissolve impurities. Hot filtration afforded 1.02 g (0,88 mmol) of 4 as a white solid. Yield: 72%; ^{1}H NMR (400 MHz, DMF-*d*$_7$) δ 9.77 (s, 4H, NH), 8.53 (s, 2H, Isophth-H), 8.40 (s, 4H, Isophth-H), 7.02 (s, 8H, Ar-H), 2.23 – 2.08 (m, 8H, Cy-H), 2.04 (s, 24H, CH_3), 1.43 – 1.23 (m, 12H, Cy-H); ^{13}C NMR (176 MHz, DMF-*d*$_7$) δ 163.71, 147.21, 139.01, 137.48, 135.40, 132.84, 126.61, 109.95, 94.02, 46.37, 45.21, 36.65, 26.32, 23.04, 18.27; HR-MS (ESI, pos. mode): m/z: calcd. for $[C_{60}H_{63}N_4O_4I_2]^+$: 1157.29332 ($[M+H]^+$); found: 1157.27579.

11’,29’-bis(4-(2,2’-6’,2”-terpyridyl)phenyl)-5’,17’,23’,35’,38’,40’,43’,45’-octamethyldispiro[cyclohexane-1,2’-7’,15’,25’,33’-tetraazaheptacylo[32.2.2.$2^{3',6'}$.$2^{16',19'}$.$2^{21',24'}$.$1^{9',13'}$.$1^{27',31'}$]hexatetraconta-3’,5’,9’,11’,13’(44’),16’,18’,21’,23’,27’,29’,31’(39’),34’,36’,37’,40’,42’,45’-octadecaene-20’,1’’-cyclohexane]-8’,14’,26’,32’-tetraone (MC). 4 (100 mg, 0.083 mmol), cesium carbonate (84 mg, 0.23 mmol) and tetrakis(triphenylphosphine)palladium (10 mg, 0.0086 mmol) were dissolved in 40 ml DMF/toluene 1:1. The mixture was heated to 60°C and 4’-(4-(4,4,5,5-tetramethyl-2-phenyl-1,3,2-dioxaborolane)phenyl)-2,2’-6’,2”-terpyridine 5 (83 mg, 0.19 mmol) was added, afterwards the temperature was kept at 60°C for 5 d. The solvent was removed under reduced pressure and the crude product was filtered through silica with dichloromethane/methanol 9:1 as the eluent. Dialysis (Spectrumlabs, MWCO 1000 Da) with dichloromethane/methanol 2:1 as the solvent afforded 53 mg (0.034 mmol) of pure product. Yield: 42%; ^{1}H NMR (500 MHz, $CDCl_3/CD_3OD$) δ 8.73 – 8.52 (m, 12H, tpy-H), 8.51 – 8.29 (m, 8H, tpy-H/ Isophth-H), 8.05 – 7.95 (m, 2H, Isophth-H), 7.89 – 7.82 (m, 4H, tpy-H), 7.81 – 7.66 (m, 4H, tpy-H), 7.38 – 7.29 (m, 4H, tpy-H), 6.96 (s, 8H, Ar-H), 2.36 – 2.24 (m, 8H, Cy-H), 2.11 (s, 24H, CH_3), 1.66 – 1.36 (m, 12H, Cy-H). Because of the low solubility of MC, it was impossible to record a ^{13}C NMR-spectrum; HR-MS (ESI, pos. mode): m/z: calcd. for $[C_{102}H_{92}N_{10}O_4]^+$: 760.86620 ($[M+2H]^+$); found: 760.86085.

The dimeric complexes ***t*BuMC$_2$Fe** and ***t*BuMC$_2$Ni** were synthesized as control compounds. The syntheses were performed according to modified literature procedures as follows.[11]

Bis(11’-*tert*-butyl-29’-(4’-(4-(2,2’-6’,2”-terpyridyl)phenyl)-5’,17’,23’,35’,38’,40’,43’,45’-octamethyldispiro[cyclohexane-1,2’-7’,15’,25’,33’-tetraazaheptacylo[32.2.2.$2^{3',6'}$.$2^{16',19'}$.$2^{21',24'}$.$1^{9',13'}$.$1^{27',31'}$]hexatetraconta-3’,5’,9’,11’,13’(44’),16’,18’,21’,23’,27’,29’,31’(39’),34’,36’,37’,40’,42’,45’-octadecaene-20’,1’’-cyclohexane]-8’,14’,26’,32’-tetraone) iron(II) tetrafluoroborate (*t*BuMC$_2$Fe). To a solution of iron(II) tetrafluoroborate hexahydrate (3.4 mg, 0.01 mmol) in 1 ml acetonitrile, monoterpyridine macrocycle 6 (25.4 mg, 0.02

mmol) dissolved in 4 ml acetonitrile was added dropwise. The reaction was allowed to stir at r.t. for 2 h and the solvent was removed under reduced pressure. Precipitation with cold diethylether afforded 11.2 mg (0.004 mmol) of pure product. Yield: 40%; ^{1}H NMR (400 MHz, DMF-d_7) δ 9.92 (s, 4H, NH), 9.51 (s, 4H, NH), 9.28 (s, 4H, tpy-H), 9.24 (d, 4H, tpy-H), 8.97 (s, 2H, Isophth-H), 8.80 (d, 4H, tpy-H), 8.68 (s, 2H, Isophth-H), 8.61 (s, 4H, Isophth-H), 8.33 (d, 4H, tpy-H), 8.19 (s, 4H, Isophth-H), 8.14 (t, 4H, tpy-H), 7.69 (d, 4H, tpy-H), 7.35 – 7.28 (m, 4H, tpy-H), 7.25 (d, *J* = 14.4 Hz, 16H, Ar-H), 2.53 – 2.40 (m, 16H, Cy-H), 2.24 (s, 24H, CH_3), 2.17 (s, 24H, CH_3), 1.71 – 1.44 (m, 24H, Cy-H). Because of the low solubility of *t*BuMC$_2$Fe, it was impossible to record a ^{13}C NMR-spectrum; HR-MS (ESI, pos. mode): m/z: calcd. for $[C_{170}H_{170}FeN_{14}O_8]^+$: 1296.13501 ($[M-2BF_4]^{2+}$); found: 1296.16720.

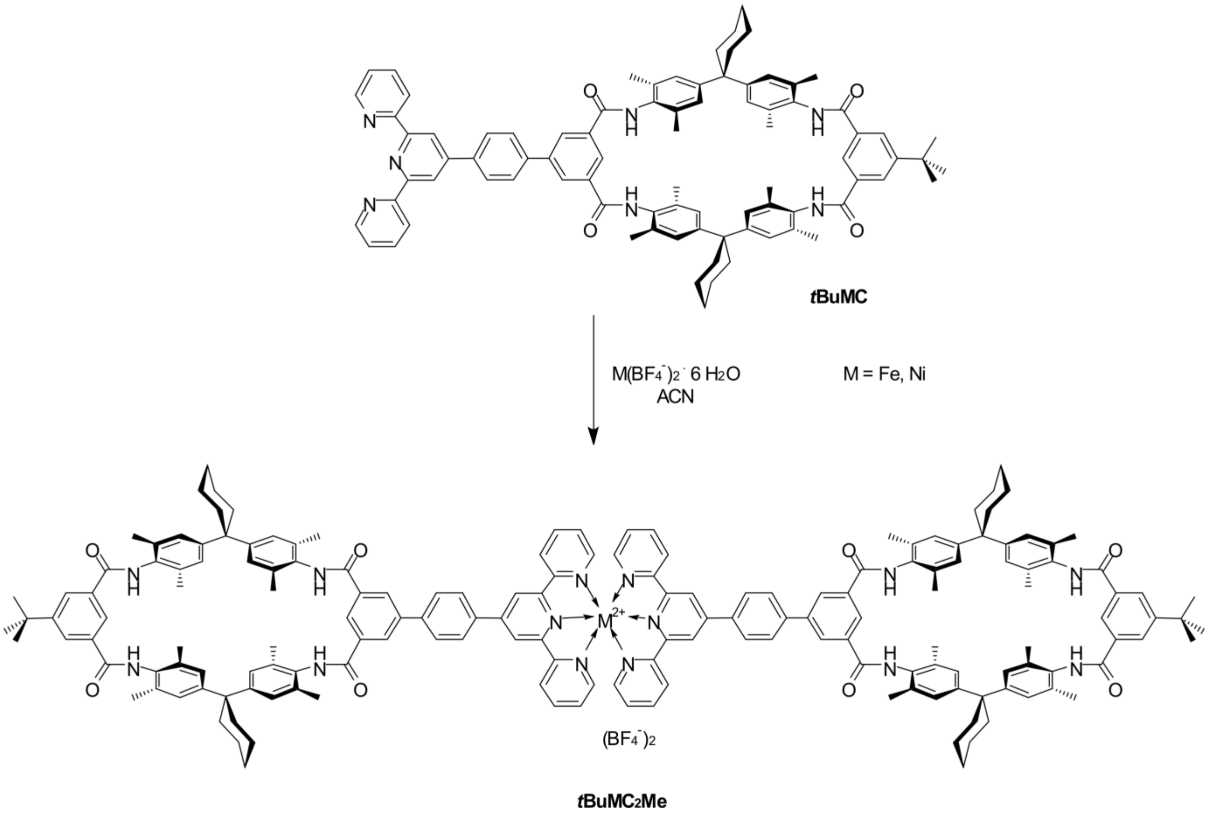

Fig. S2: Synthesis of the control complexes ***t*BuMC$_2$Fe** and ***t*BuMC$_2$Ni**

Bis(11’-*tert*-butyl-29’-(4’-(4-(2,2’-6’,2”-terpyridyl)phenyl)-5’,17’,23’,35’,38’,40’,43’,45’-octamethyldispiro[cyclohexane-1,2’-7’,15’,25’,33’-tetraazaheptacylo[32.2.2.2$^{3’,6’}$.2$^{16’,19’}$.2$^{21’,24’}$.1$^{9’,13’}$.1$^{27’,31’}$]hexatetraconta-3’,5’,9’,11’,13’(44’),16’,18’,21’,23’,27’, 29’,31’(39’),34’,36’,37’,40’,42’,45’-octadecaene-20’,1’’-cyclohexane]-8’,14’,26’,32’-tetraone) nickel(II) tetrafluoroborate (*t*BuMC$_2$Ni) was synthesized accordingly, using nickel(II) tetrafluoroborate hexahydrate as the metal source. Yield: 48%; ^{1}H NMR (400 MHz, DMF-d_7) δ 9.91 (s, 4H, NH), 9.57 (s, 4H, NH), 9.30 (s, 4H, Isophth-H), 9.05 (s, 2H, Isophth-H), 8.69 (s, 2H, Isophth-H), 8.20 (s, 4H, Isophth-H), 7.27 (d, *J* = 17.7 Hz, 16H, Ar-H), 2.49 (s, 8H, Cy-H), 2.28 (s, 24H, CH_3), 2.19 (s, 24H, CH_3), 1.59 (d, *J* = 43.2 Hz, 24H, Cy-H). Because of the para-magnetic nature of the Ni(II) complex, the signals of the terpyridine protons were not observed; HR-MS (ESI, pos. mode): m/z: calcd. for $[C_{170}H_{170}NiN_{14}O_8]^+$: 1297.63571 ($[M-2BF_4]^{2+}$); found: 1297.61186.

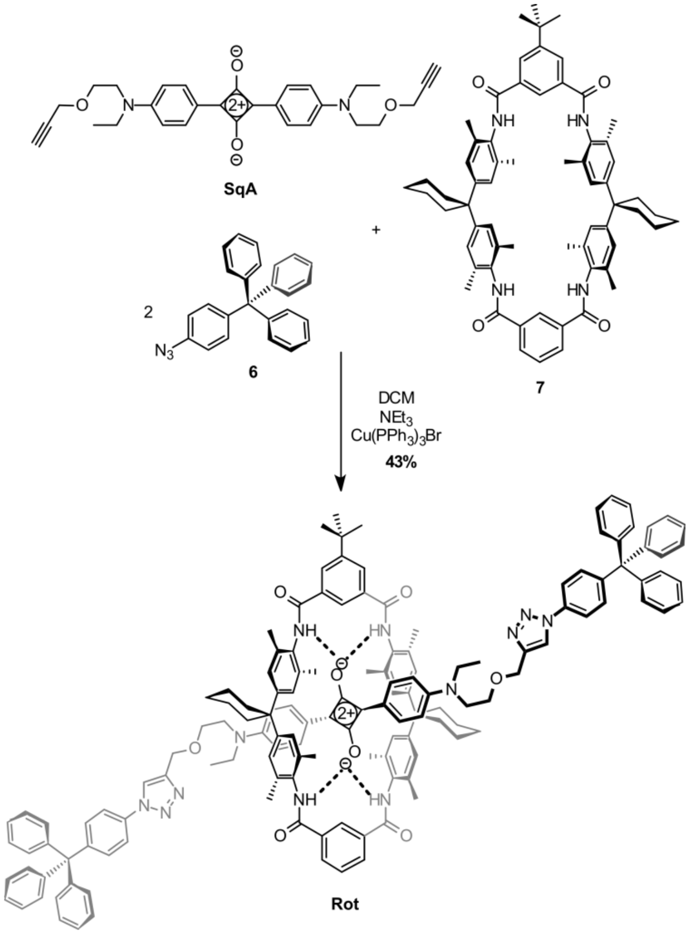

Fig. S3: Synthesis of the control rotaxane **Rot**.

Rot was synthesized as control compound according to modified literature procedures as follows. The starting products **6**, **7** and **SqA** are literature-known compounds.[10,12]

Control rotaxane Rot. A solution of **6** (61.44,g, 0.17 mmol), **7** (22.11 mg, 0.0023 mmol), **SqA** (24.43 mg, 0.05 mmol), Cu(PPh$_3$)$_3$Br (8 mg, 0.0086 mmol) and triethylamine (17 µl, 0.12 mmol) in 4 ml dichloromethane was stirred at 35°C for 2d. The solvent was removed under reduced pressure. Preparative TLC on silica with dichloromethane/methanol (96:4) as the eluent afforded 22 mg (0.01 mmol) of pure product. Yield: 43%; ^{1}H NMR (400 MHz, CDCl$_3$) δ 9.32 (s, 1H, Isophth-H), 9.13 (s, 1H, Isophth-H), 8.78 (s, 2H, NH), 8.72 (s, 2H, NH), 8.40 (d, J = 1.3 Hz, 2H, Isophth-H), 8.34 (dd, J = 7.9, 1.3 Hz, 2H, Isophth-H), 7.93 (s, 2H, Triazol-H), 7.87 (d, J = 9.1 Hz, 4H, Ar-H$_{axle}$), 7.68 (t, J = 7.8 Hz, 1H, Isophth-H), 7.57 (d, J = 8.7 Hz, 4H, Ar-H$_{axle}$), 7.40 (d, J = 8.9 Hz, 4H, Ar-H$_{axle}$), 7.27 – 7.19 (m, J = 7.4, 3.3 Hz, 30H, Stopper-H), 6.75 (s, 8H, Ar-H$_{cycle}$), 6.65 (d, J = 9.2 Hz, 4H, Ar-H$_{axle}$), 4.66 (s, 4H, CH$_2$), 3.78 (t, J = 5.7 Hz, 4H; CH$_2$), 3.69 – 3.64 (m, 4H, CH$_2$), 3.57 (m, 4H, CH$_2$), 2.23 – 2.14 (m, J = 16.4 Hz, 8H, Cy-H), 2.03 (s, 24H, Ar-CH$_3$), 1.62 – 1.50 (m, 12H, Cy-H), 1.44 (s, 9H, tertButyl-H), 1.42 – 1.38 (m, 6H, CH$_{3,axle}$); HR-MS (ESI, pos. mode): m/z: calcd. for [C$_{144}$H$_{144}$N$_{12}$O$_8$]$^+$: 1085.06257 ([M+2H]$^{2+}$); found: 1085.15730.

Original NMR, UV/Vis and Mass Spectra of New Compounds

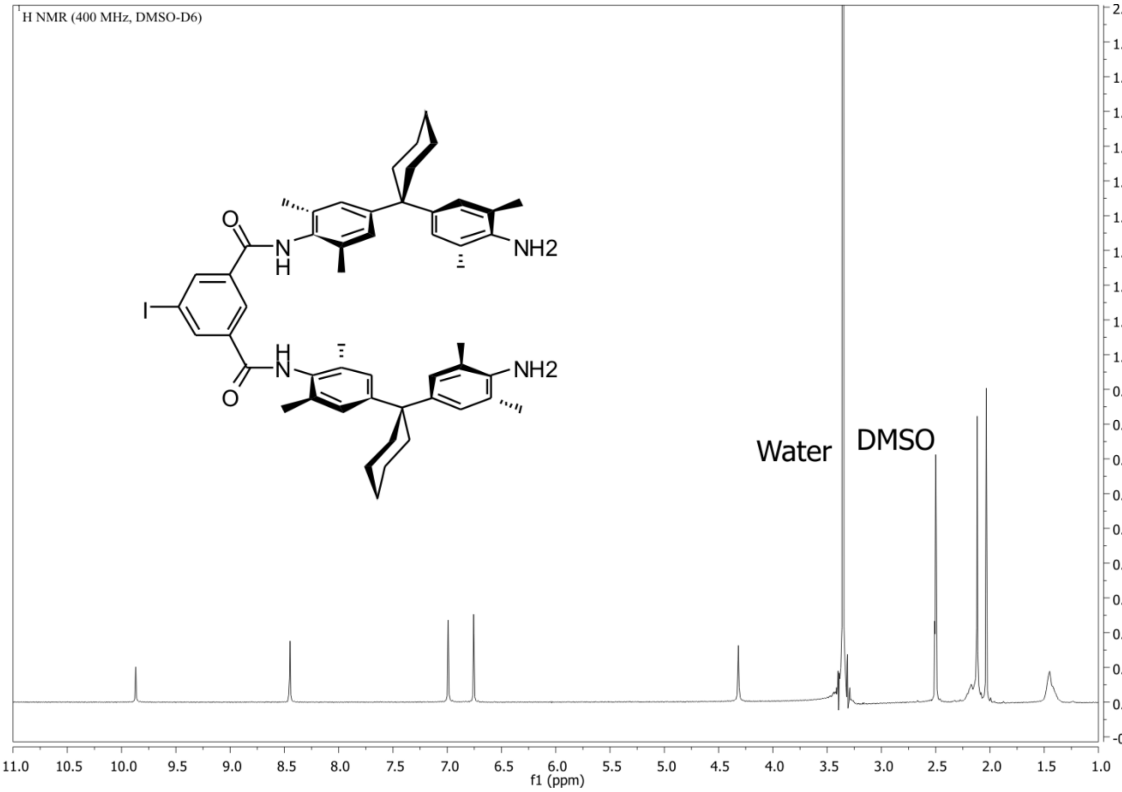

Fig. S4: ^{1}H NMR spectrum of **3**.

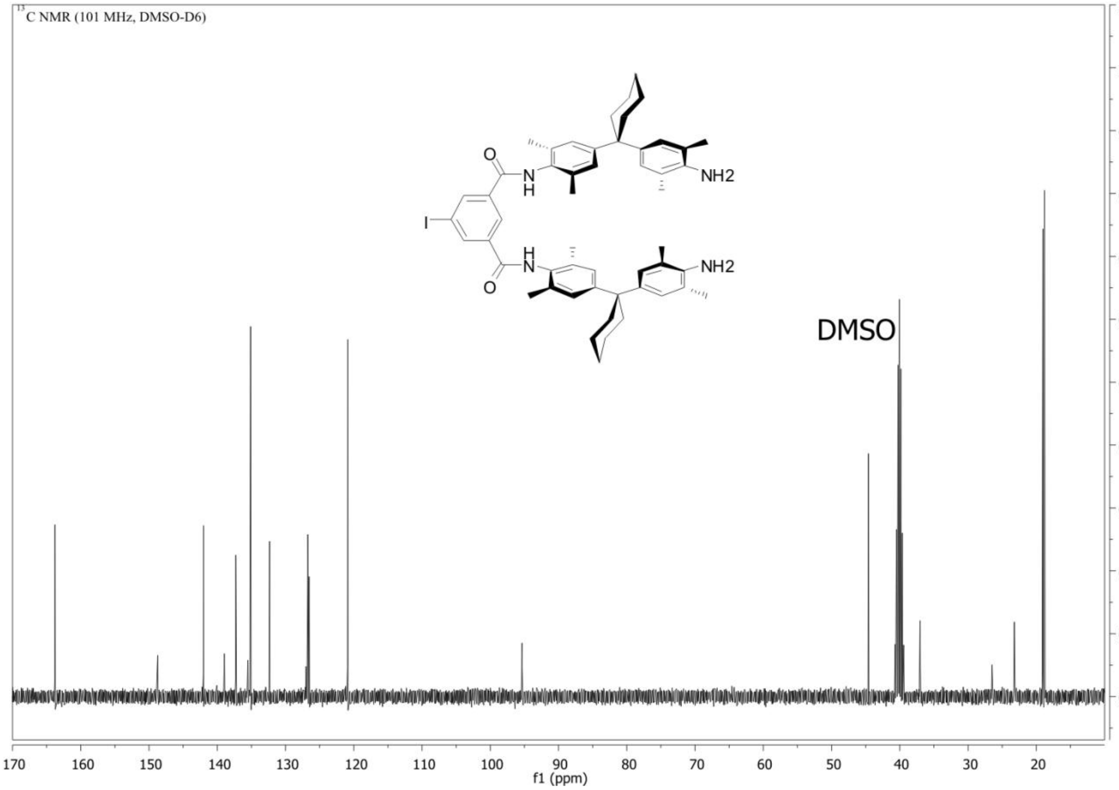

Fig. S5: ^{13}C NMR spectrum of **3**.

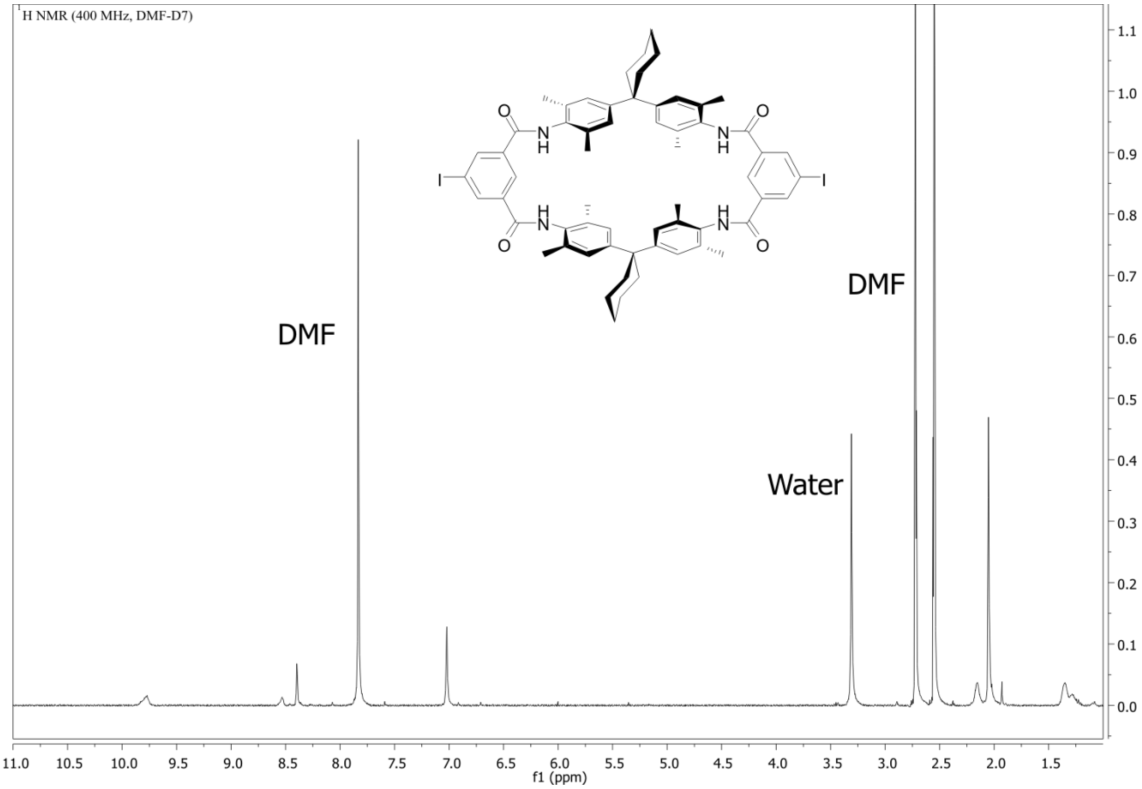

Fig. S6: ^{1}H NMR spectrum of **4**.

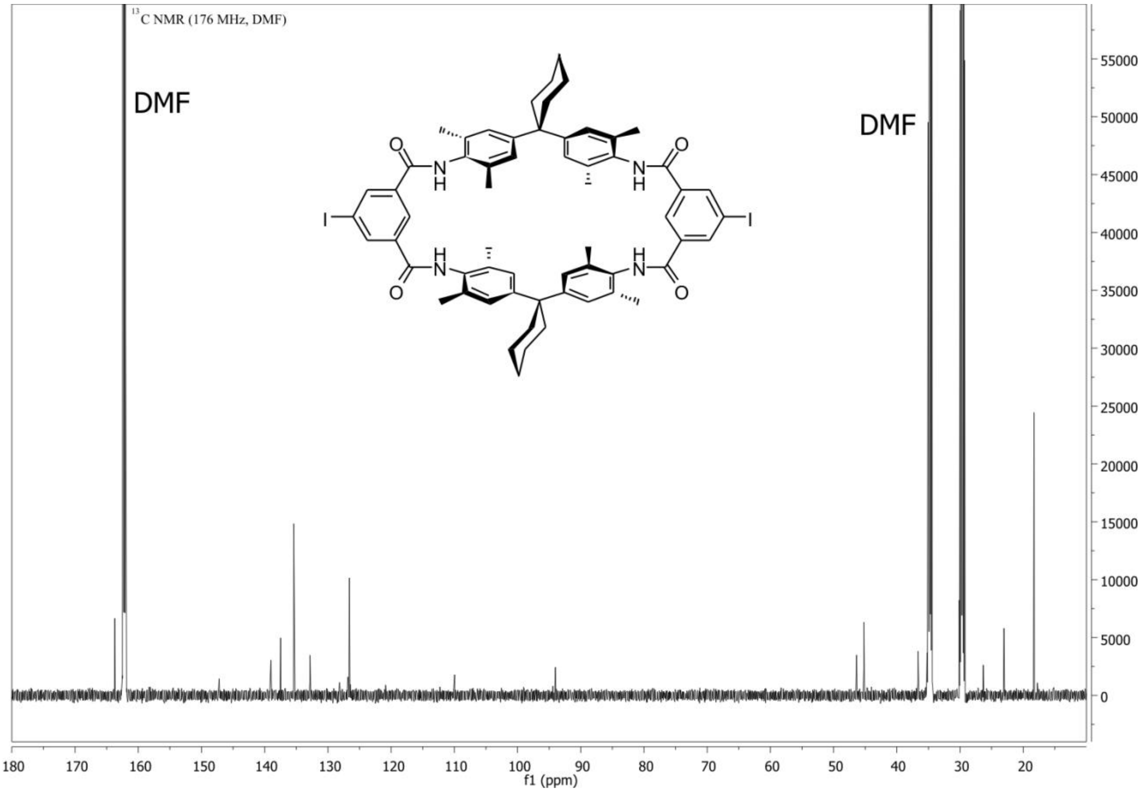

Fig. S7: ^{13}C NMR spectrum of **4**.

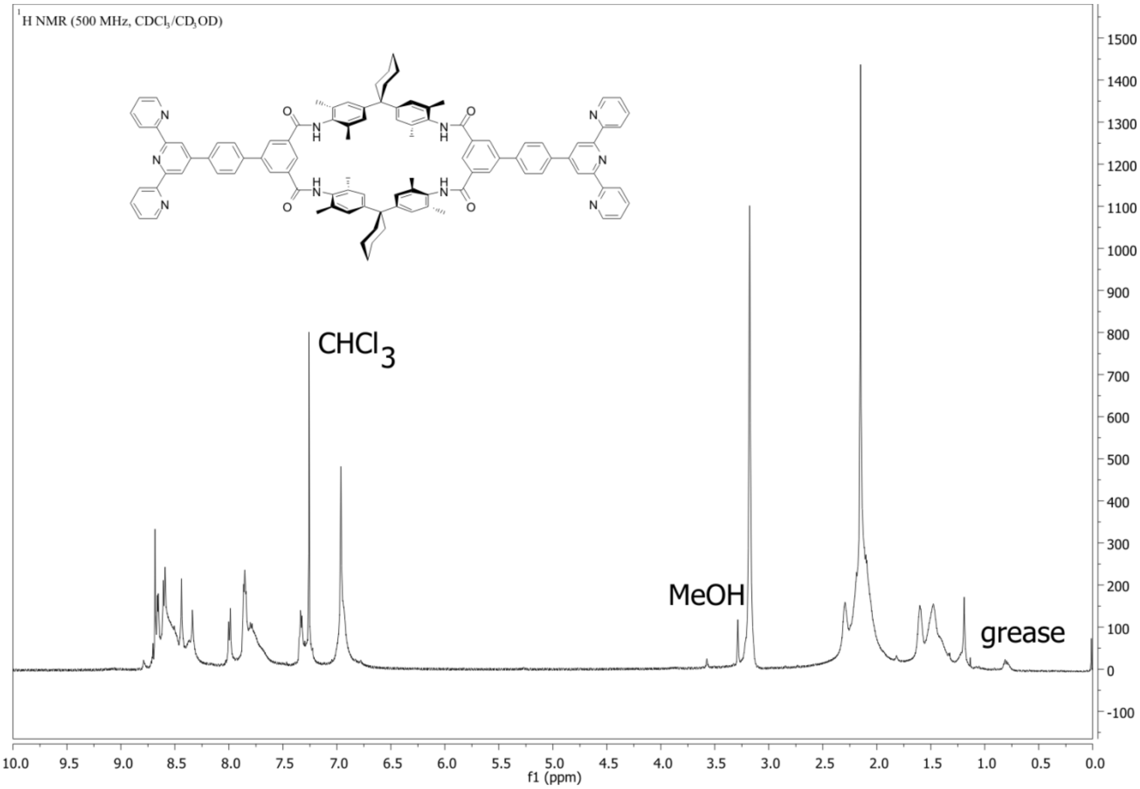

Fig. S8: ^{1}H NMR spectrum of **MC**.

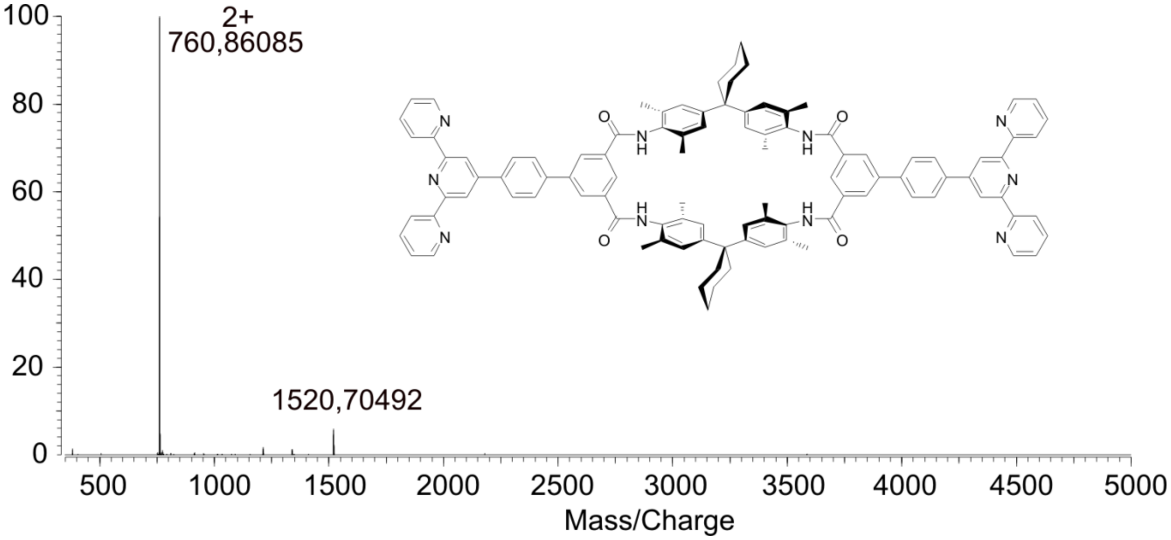

Fig. S9: ESI-FTICR mass spectrum of **MC**.

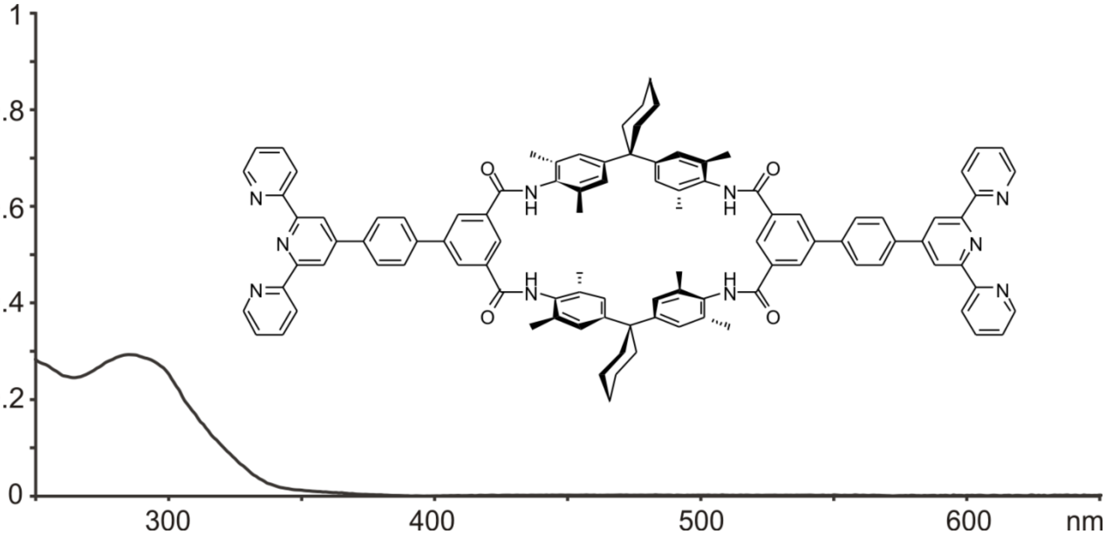

Fig. S10: UV/Vis spectrum of **MC** in dichloromethane.

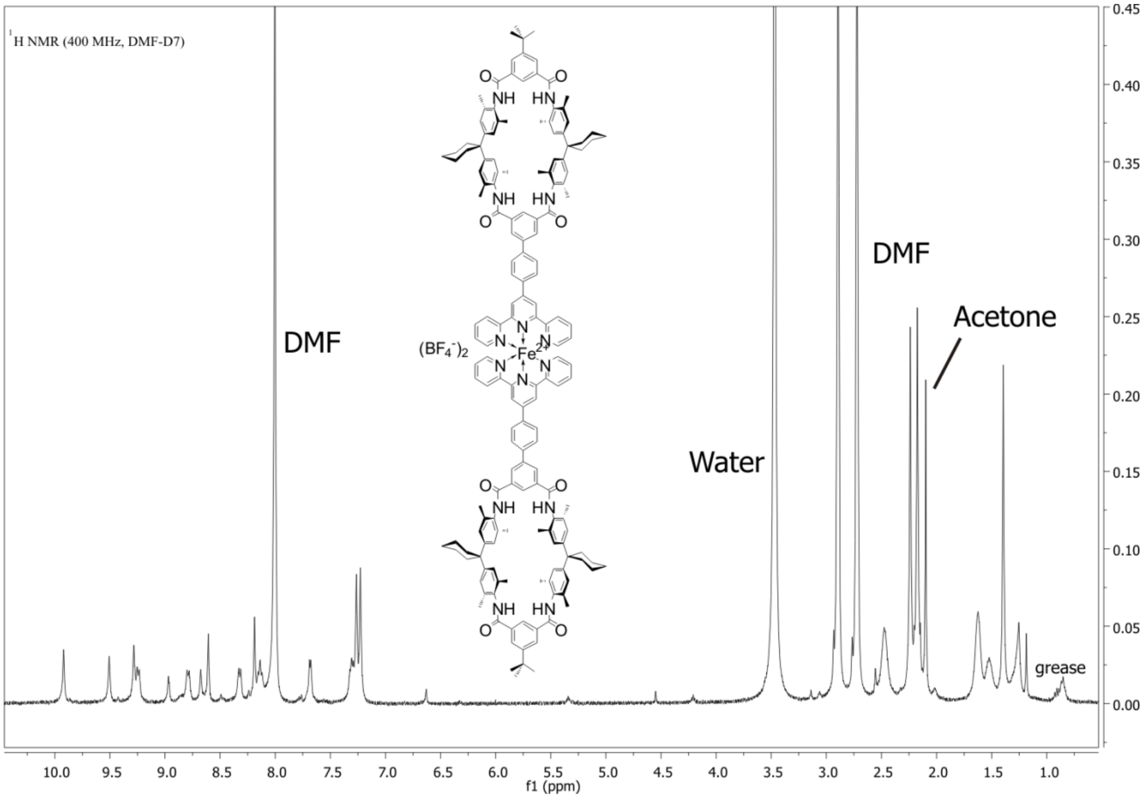

Fig. S11: ^{1}H NMR spectrum of ***t*BuMC$_2$Fe.**

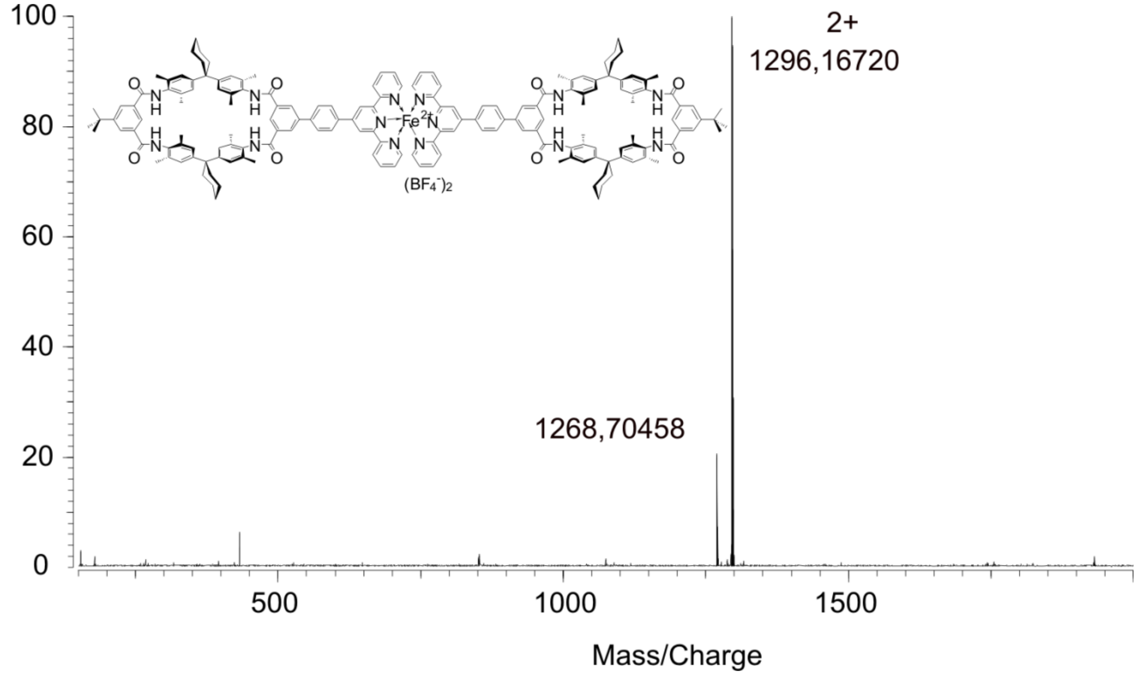

Fig. S12: ESI-FTICR mass spectrum of ***t*BuMC$_2$Fe**, the signal at m/z 1268,70458 corresponds to [**tbuMC**+H]$^+$.

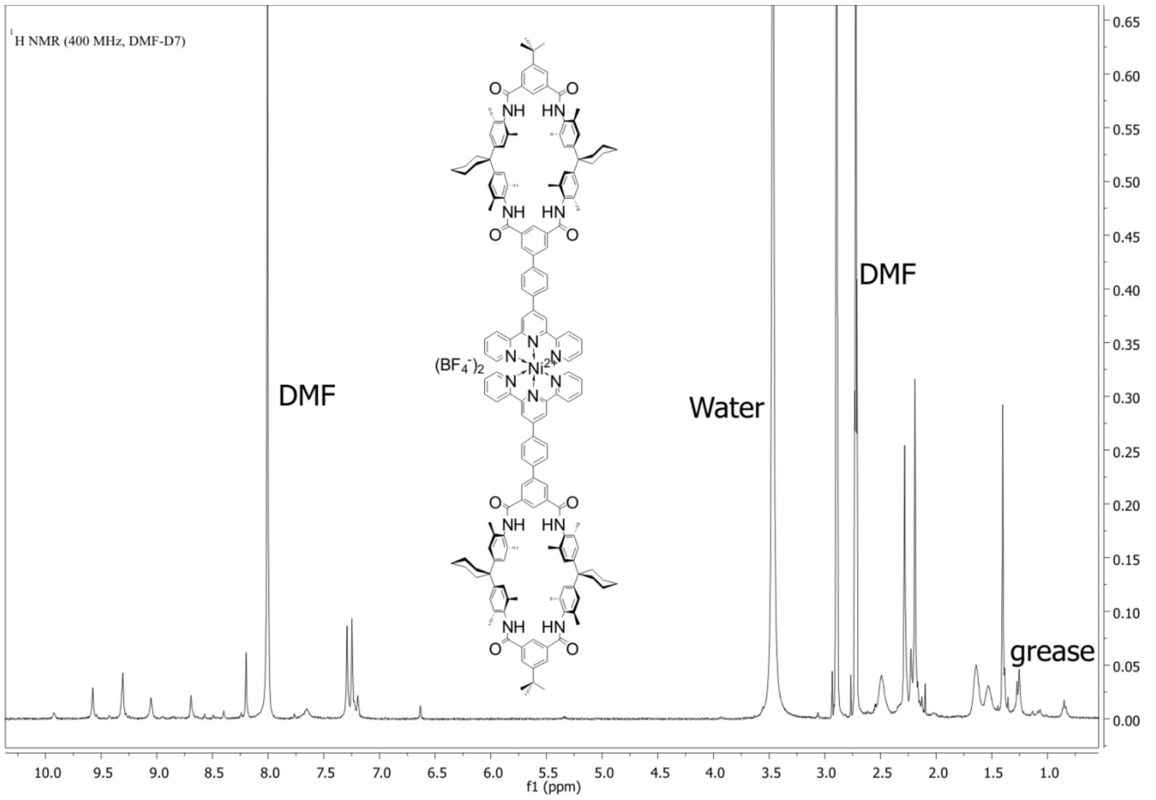

Fig. S13: ^{1}H NMR spectrum of ***t*BuMC$_2$Ni**.

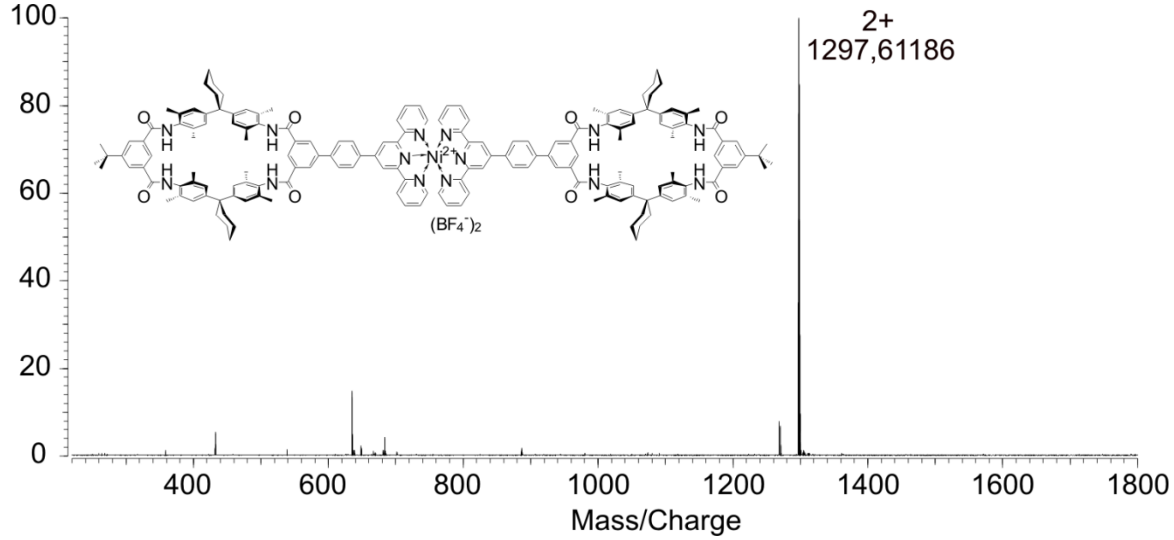

Fig. S14: ESI-FTICR mass spectrum of ***t*BuMC$_2$Ni**.

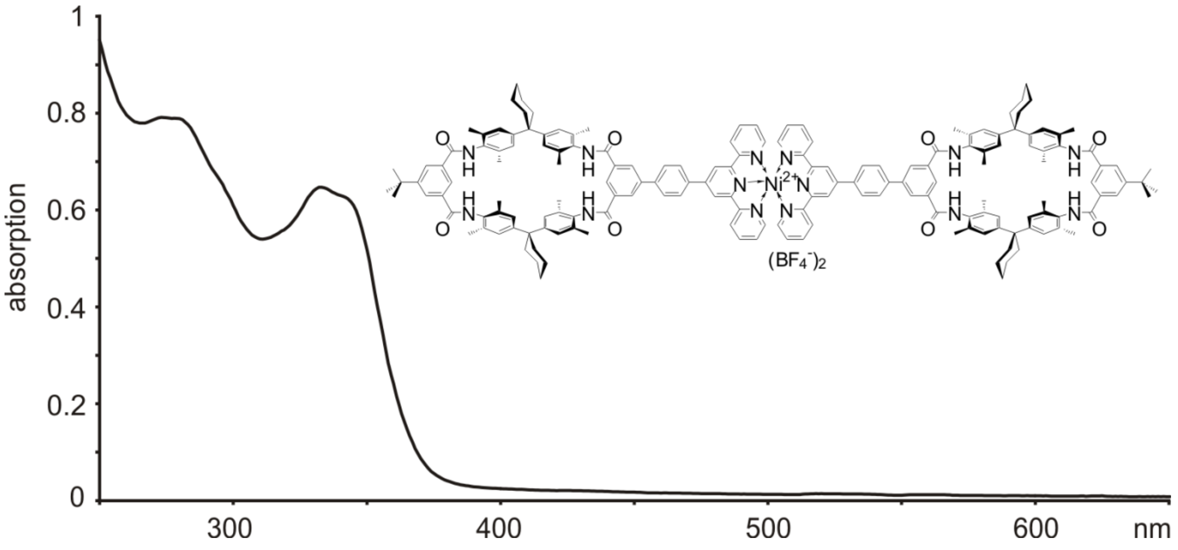

Fig. S15: UV/Vis spectrum of ***t*BuMC$_2$Ni** in ethanol.

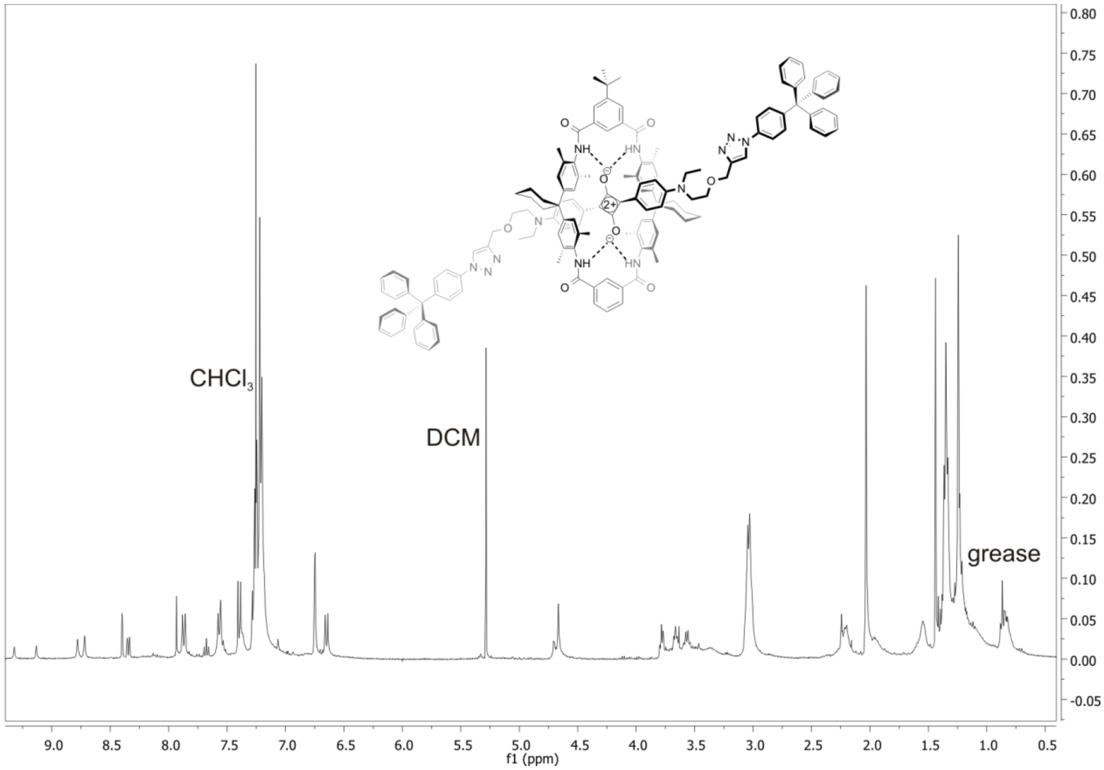

Fig. S17: ^{1}H NMR spectrum of **Rot**.

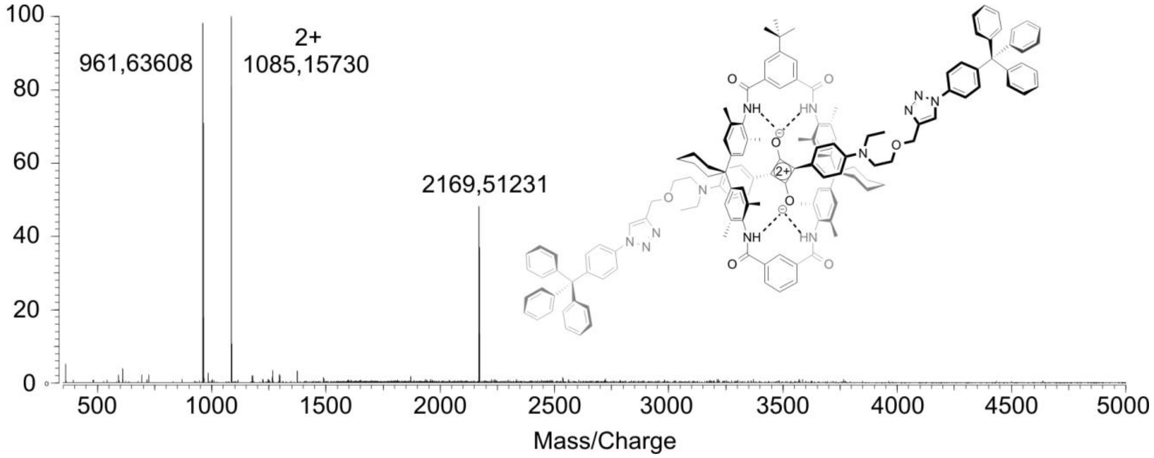

Fig. S17: ESI-FTICR mass spectrum of **Rot**, the free macrocycle was observed as a fragment at m/z 961.63608.

Additional XPS and Transmission UV/Vis Spectroscopy Data

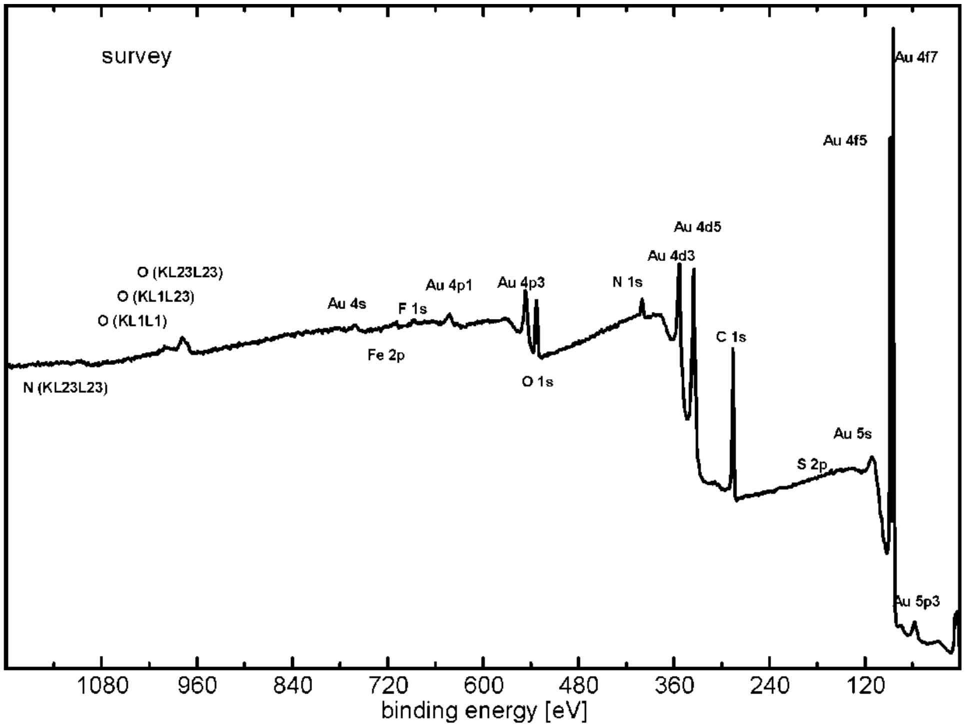

Fig. S18: XP Survey spectrum of **TDT**/**DT** 1/3 –(Fe-**MC**)$_2$.

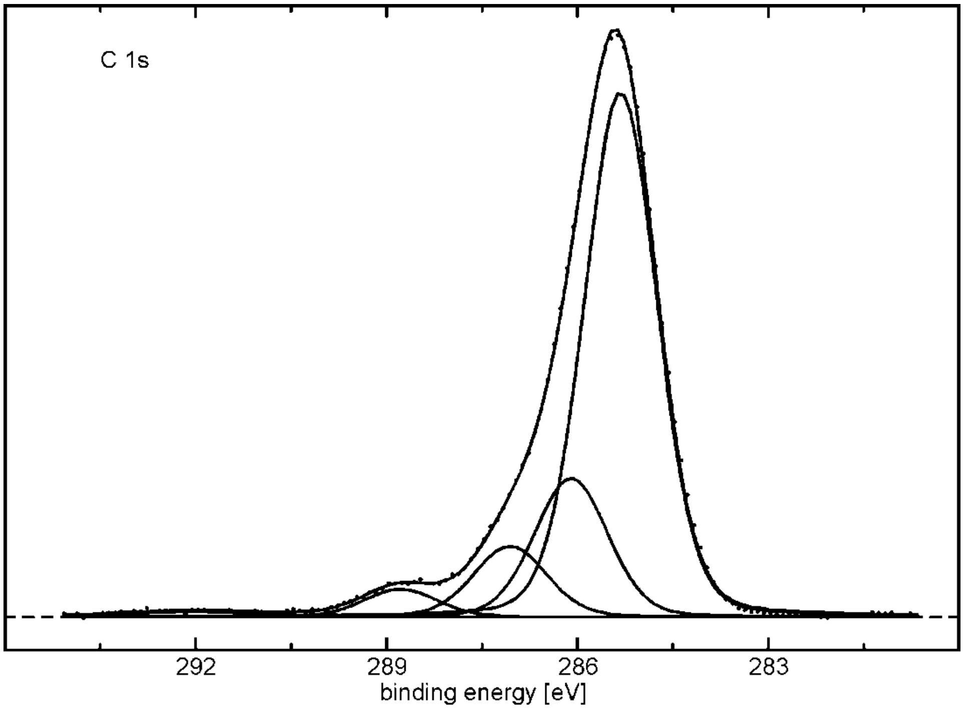

Fig. S19: XP C 1s core-level spectrum of **TDT**/**DT** 1/3 –(Fe-**MC**)$_2$.

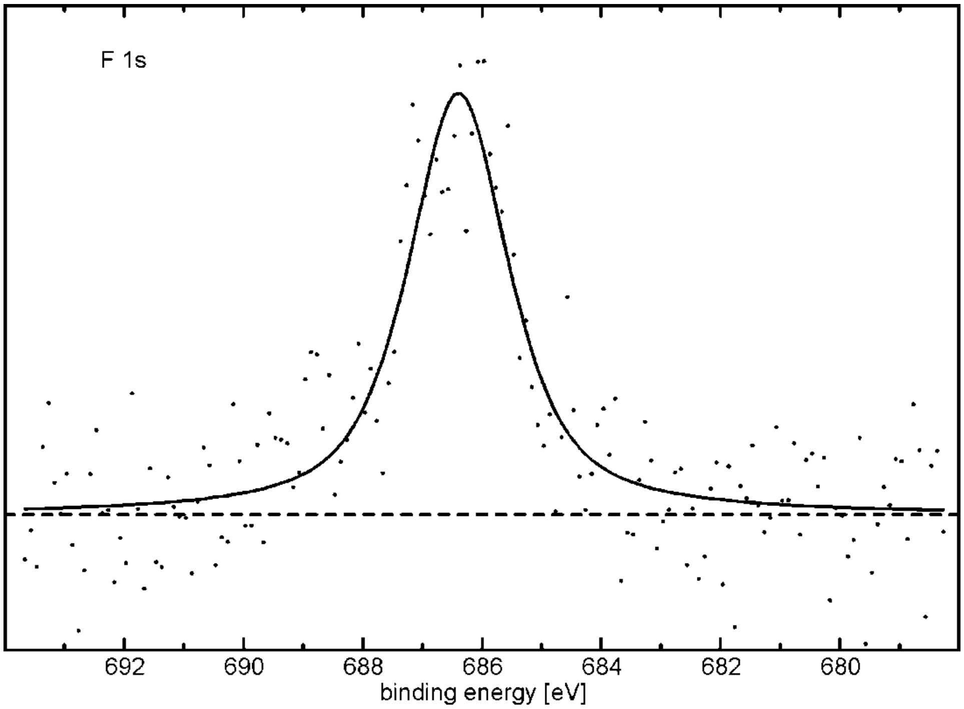

Fig. S20: XP F 1s core-level spectrum of **TDT**/**DT** 1/3 –(Fe-**MC**)$_2$.

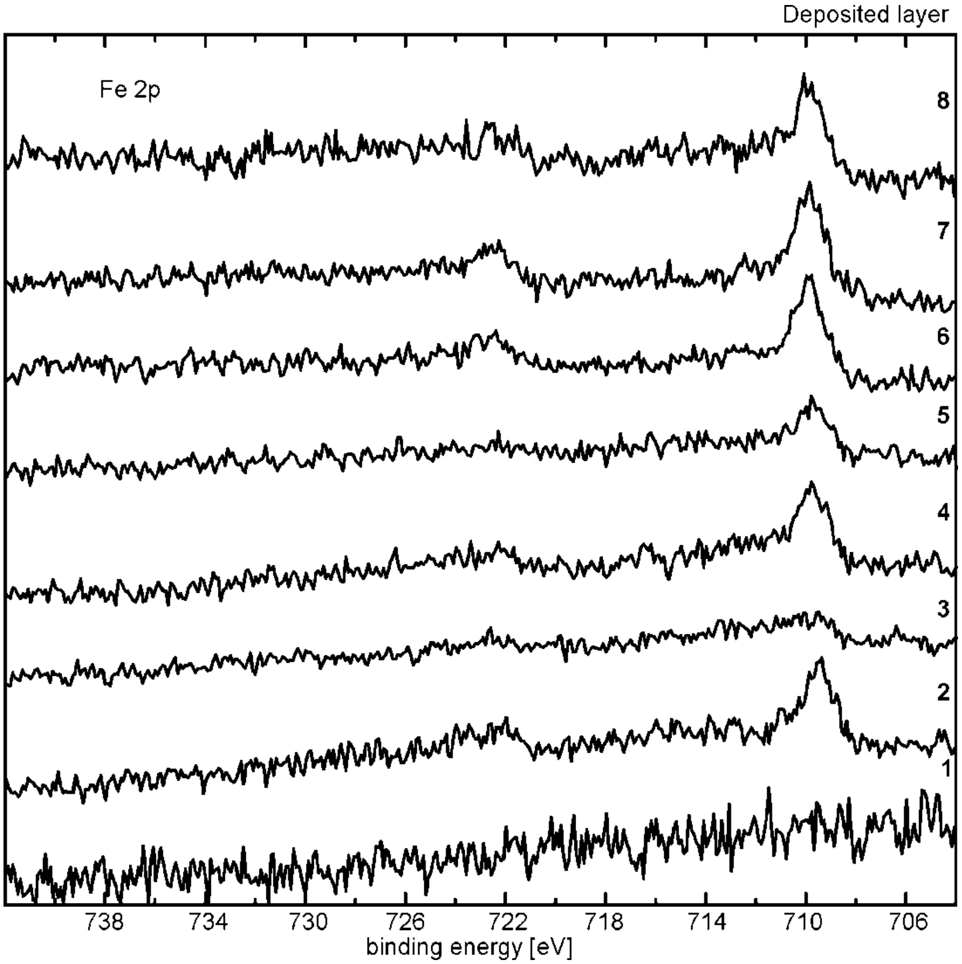

Fig. S21: XP Fe 2p core-level spectrum of **TDT**/**DT** 1/3-(Fe-**MC**) multilayer.

An alternating increase and decrease of the following N 1s peak are ratios of non-complexed terpyridine (signal at ~399.6 eV) and complexed terpyridine/amide nitrogen (both appear together at ~ 400.8 eV) species support the deposition of Fe(II) and **MC** as described in the main text.

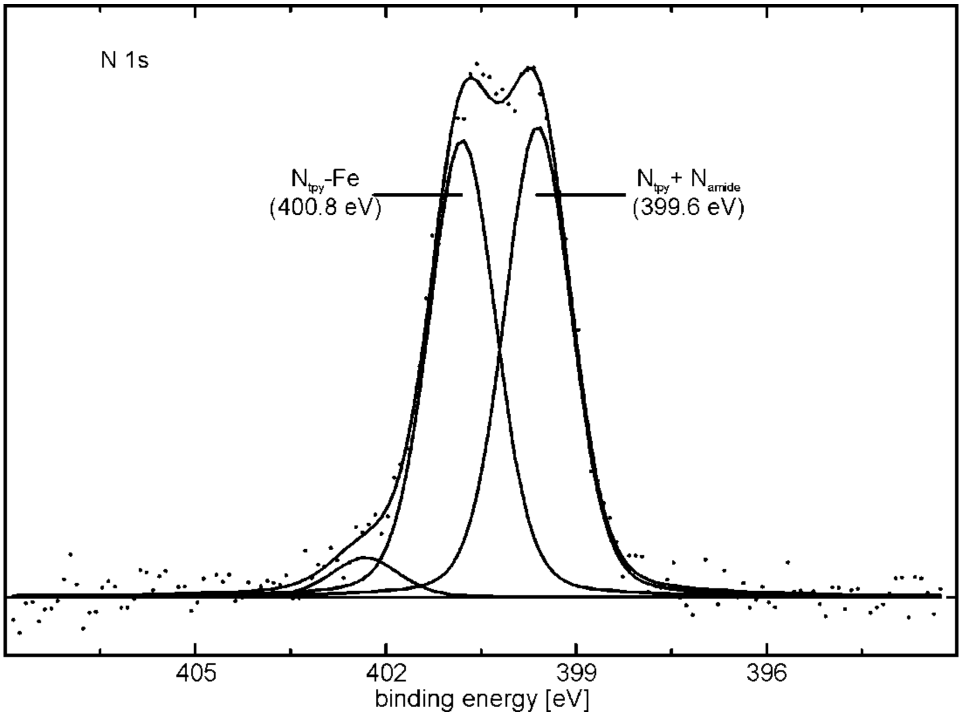

Fig. S22: XP N 1s core-level spectrum of **TDT**/**DT** 1/3 –(Fe-**MC**)$_2$. The component at higher BE 400.8 eV can be assigned to complexed terpyridine whereas the component at 399.6 eV is assigned to non-complexed terpyridine and amide nitrogen.

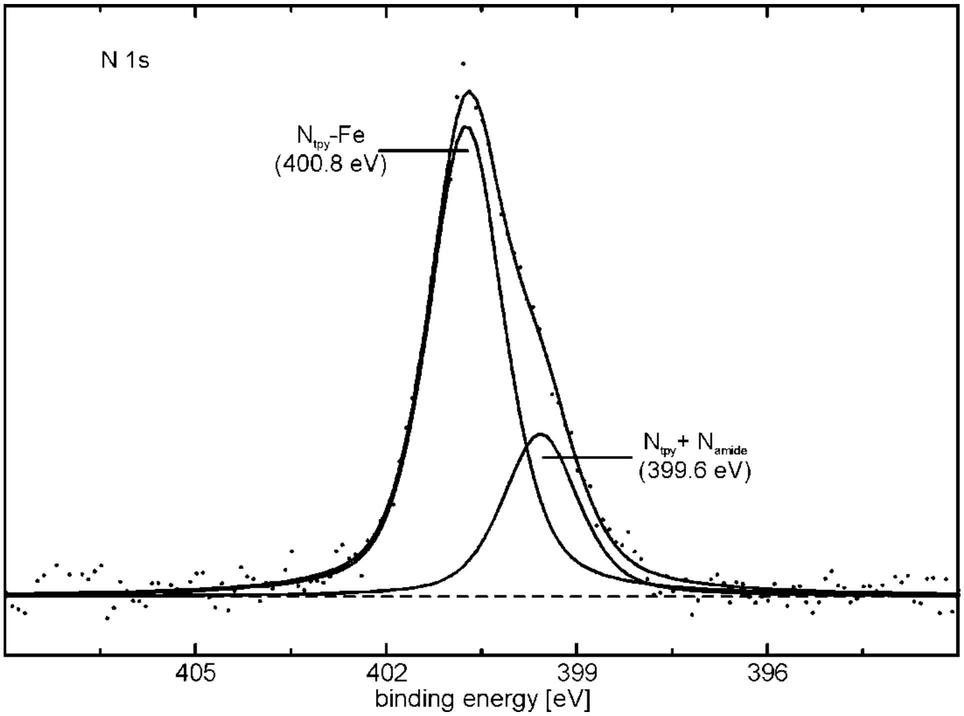

Fig. S23: XP N 1s core-level spectrum of **TDT**/**DT** 1/3 –(Fe-**MC**)$_2$Fe. The component at higher BE 400.8 eV can be assigned to complexed terpyridine whereas the component at 399.6 eV is assigned to non-complexed terpyridine and amide nitrogen.

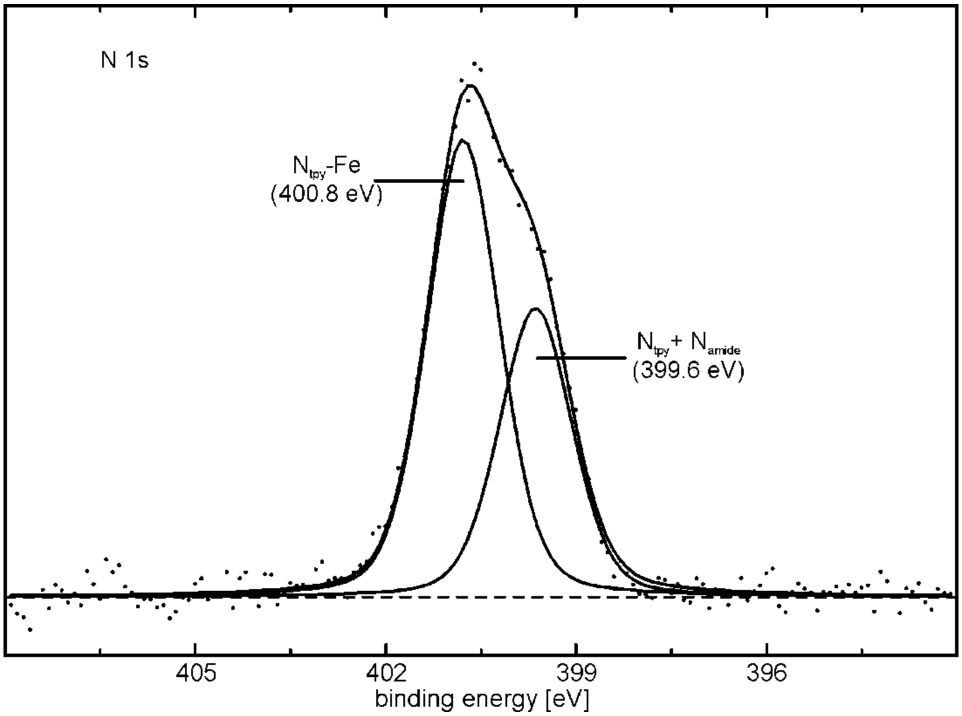

Fig. S24: XP N 1s core-level spectrum of **TDT**/**DT** 1/3 –(Fe-**MC**)$_3$. The component at higher BE 400.8 eV can be assigned to complexed terpyridine whereas the component at 399.6 eV is assigned to non-complexed terpyridine and amide nitrogen.

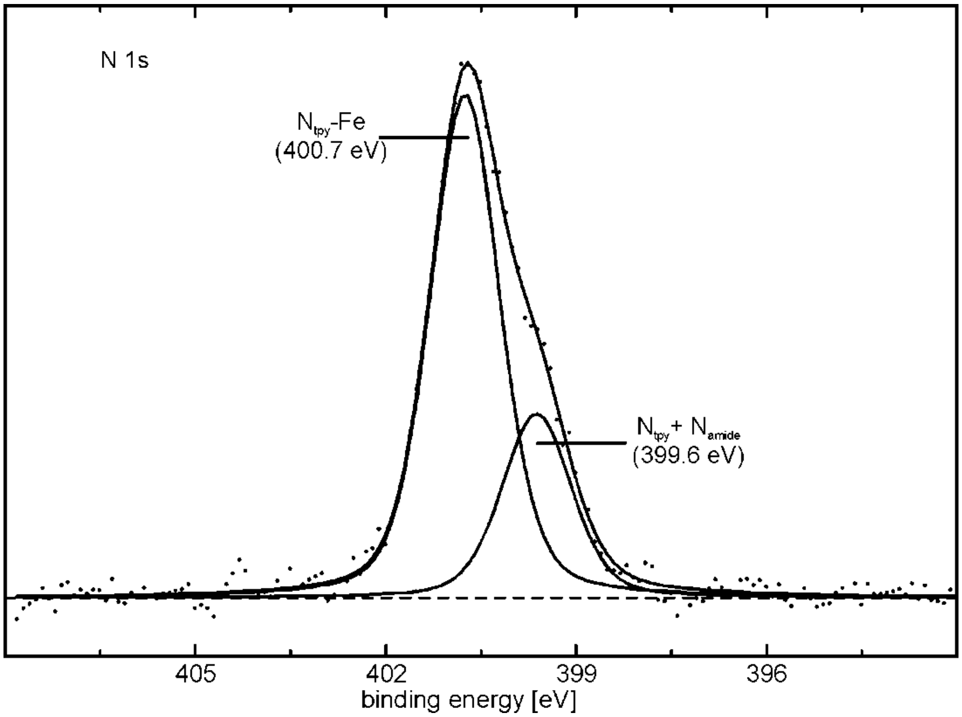

Fig. S25: XP N 1s core-level spectrum of **TDT**/**DT** 1/3 –(Fe-**MC**)$_3$Fe. The component at higher BE 400.7 eV can be assigned to complexed terpyridine whereas the component at 399.6 eV is assigned to non-complexed terpyridine and amide nitrogen.

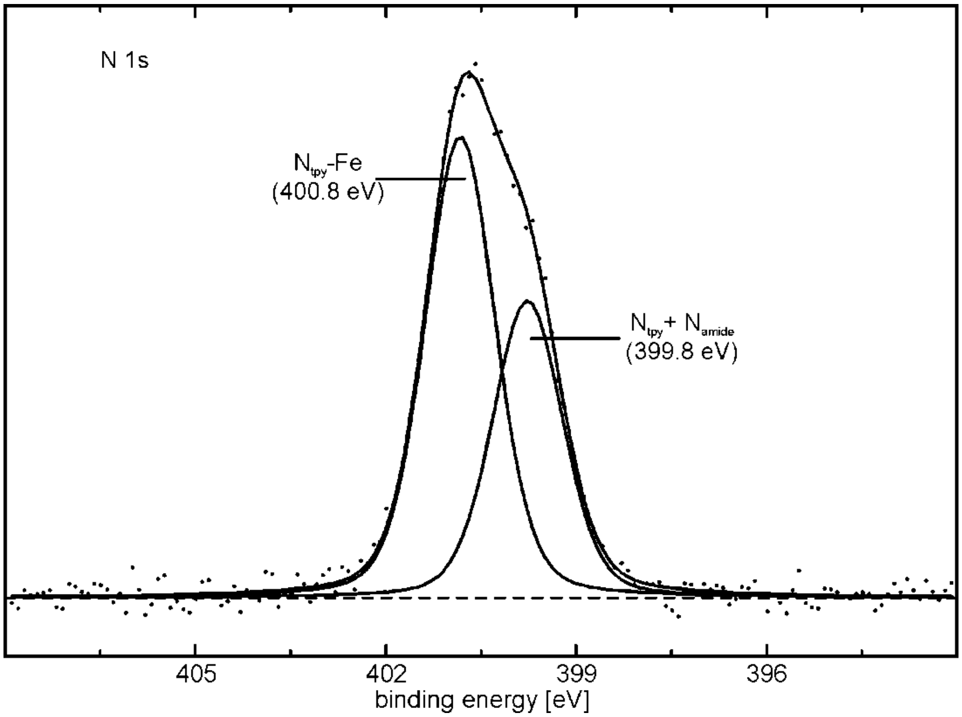

Fig. S26: XP N 1s core-level spectrum of **TDT**/**DT** 1/3 –(Fe-**MC**)$_4$. The component at higher BE 400.8 eV can be assigned to complexed terpyridine whereas the component at 399.8 eV is assigned to non-complexed terpyridine and amide nitrogen.

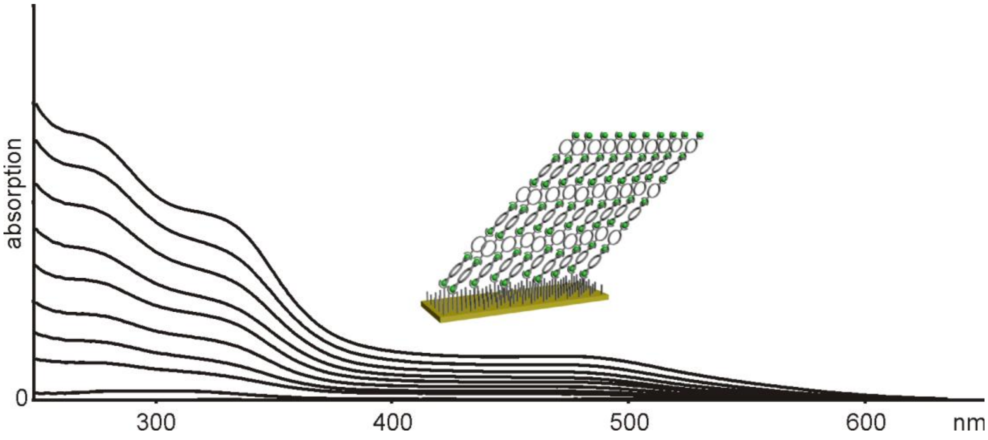

Fig. S27: Transmission-UV/Vis spectra of successful multilayer formation with **MC** and Ni(II) ions up to nine macrocycles, recorded after each macrocycle deposition.

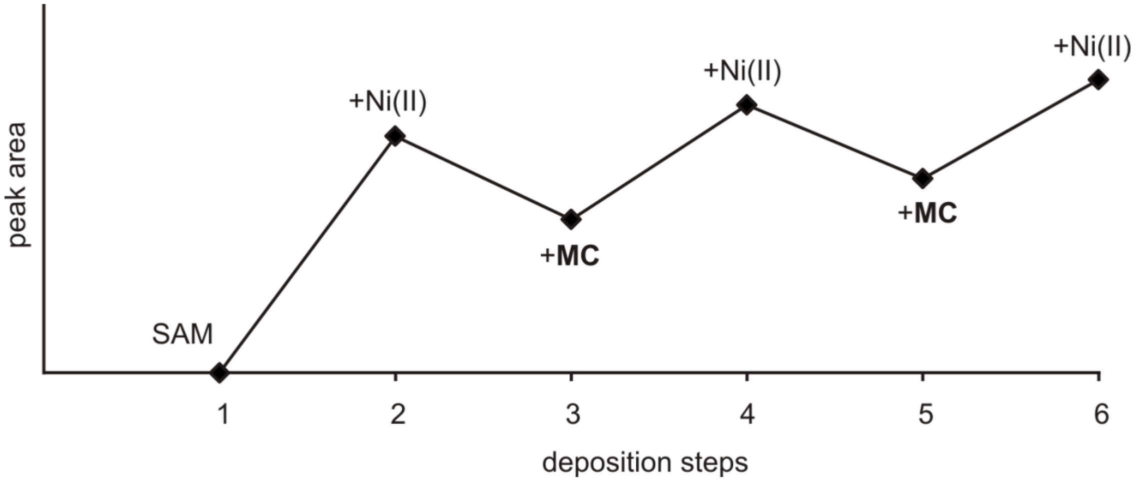

Fig. S28: Ni 2p3 (BE = 856.5 eV) peak areas obtained from XPS experiments after each deposition step.

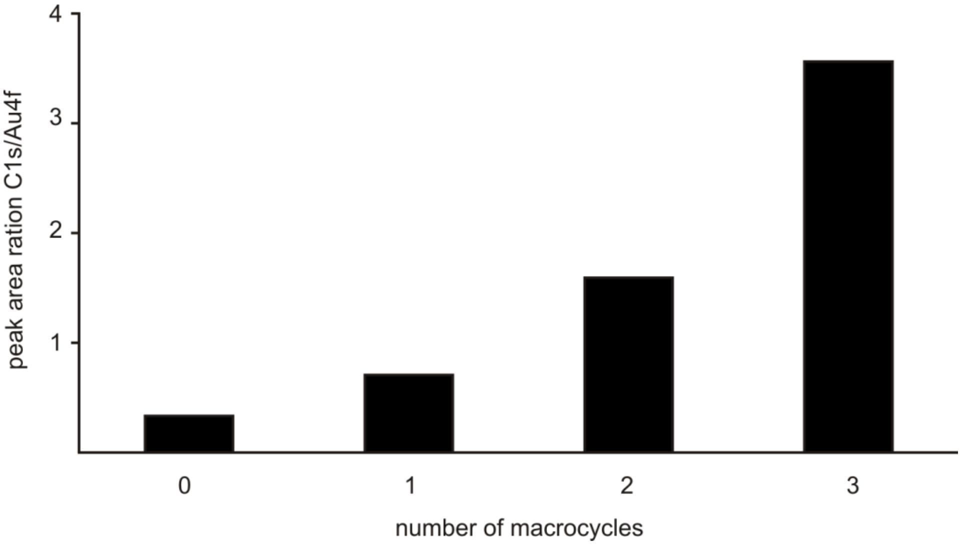

Fig. S29: XPS C/Au ratios determined after each macrocycle deposition of successful multilayer formation with **MC** and Ni(II) ions up to 3 macrocycles.

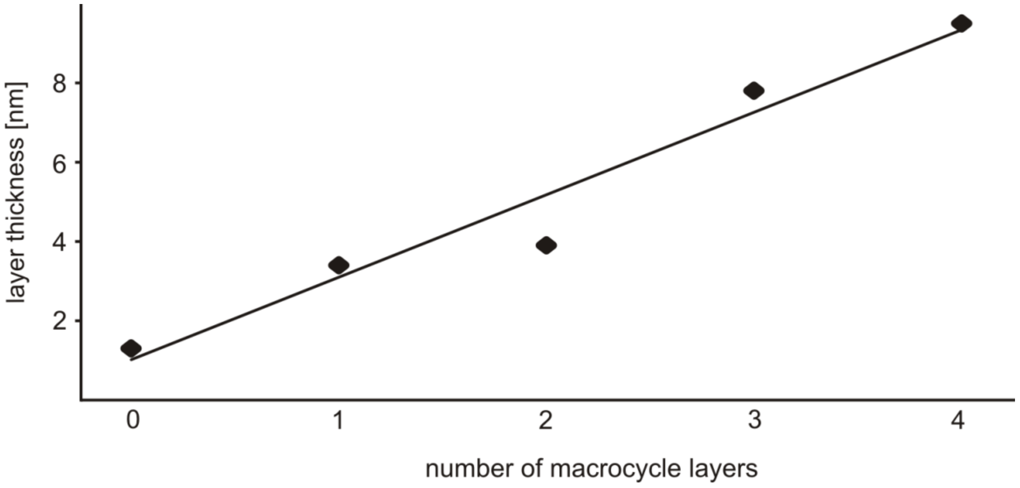

Fig. S30: Plot of layer thickness derived from XPS data over the number of deposited macrocycles of successful multilayer formation with **MC** and Ni(II) ions up to 4 macrocycles.

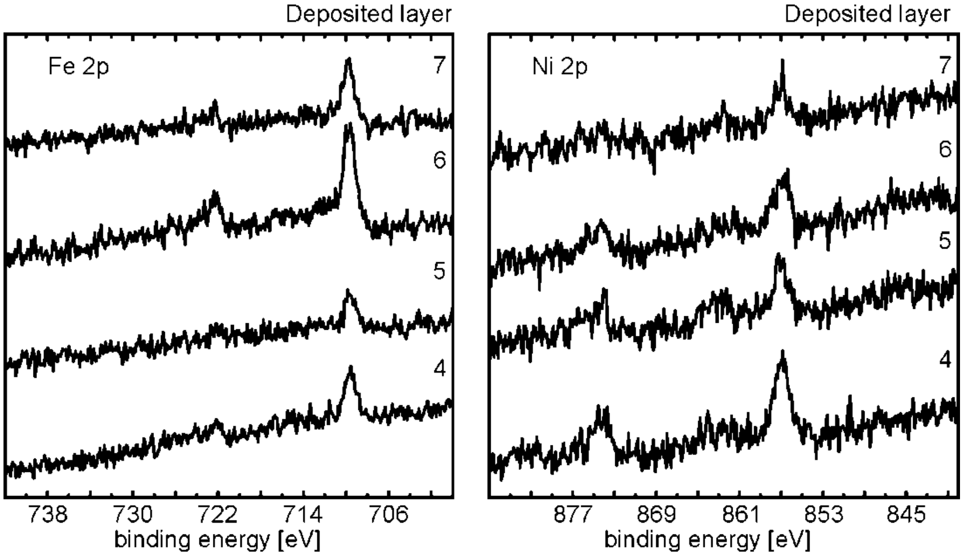

Fig. S31: XP Fe 2p and Ni 2p core-level spectra of **TDT**/**DT** 1/3 –(Fe-**MC**-Ni-**MC**) multilayer normalized to the pre-signal region.

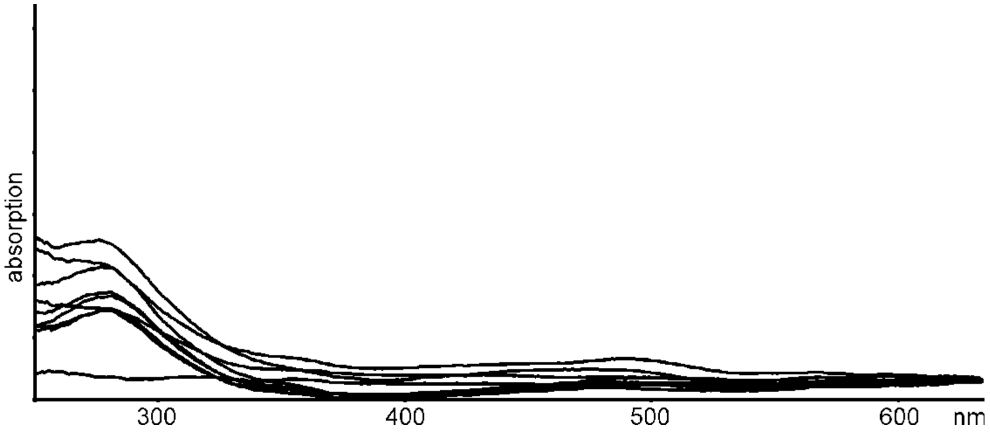

Fig. S32: Transmission-UV/Vis spectra of unsuccessful multilayer formation with **MC** and Zn(II) ions up to nine macrocycles, recorded after each macrocycle deposition. The Zn(II)-terpyridine complexes are reversible and therefore no layer growth can be observed.

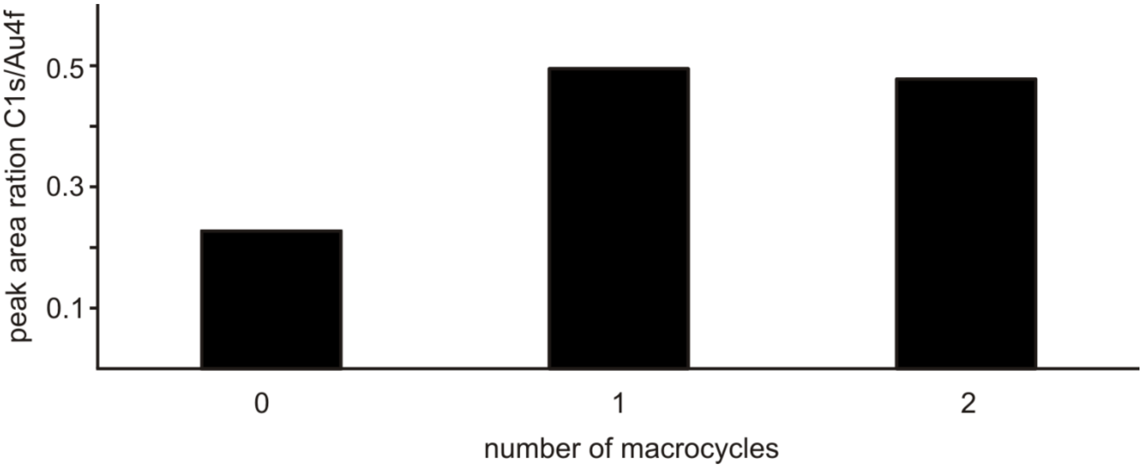

Fig. S33: XPS C/Au ratios determined after each macrocycle deposition of unsuccessful multilayer formation with **MC** and Zn(II) ions.

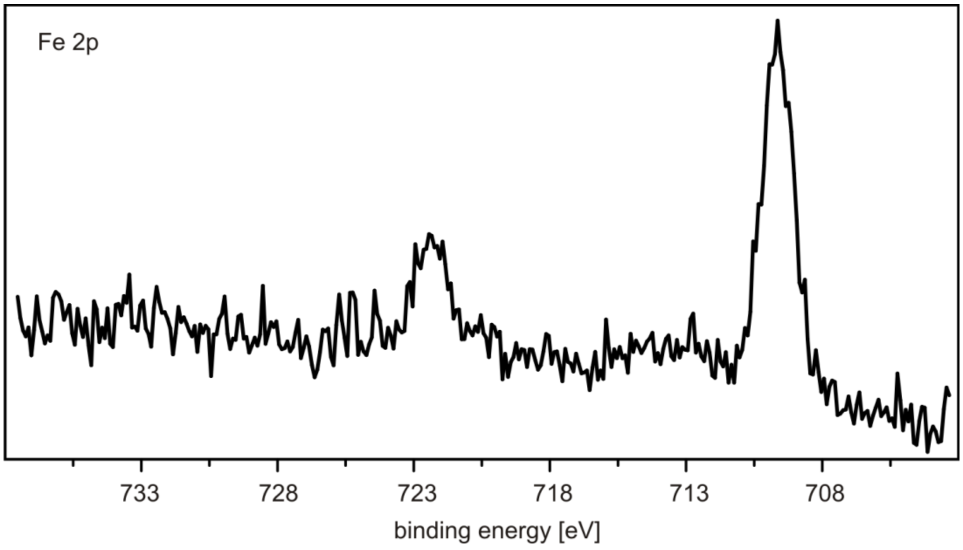

Fig. S34: Fe 2p core level spectrum of ***t*BuMC$_2$Fe**.

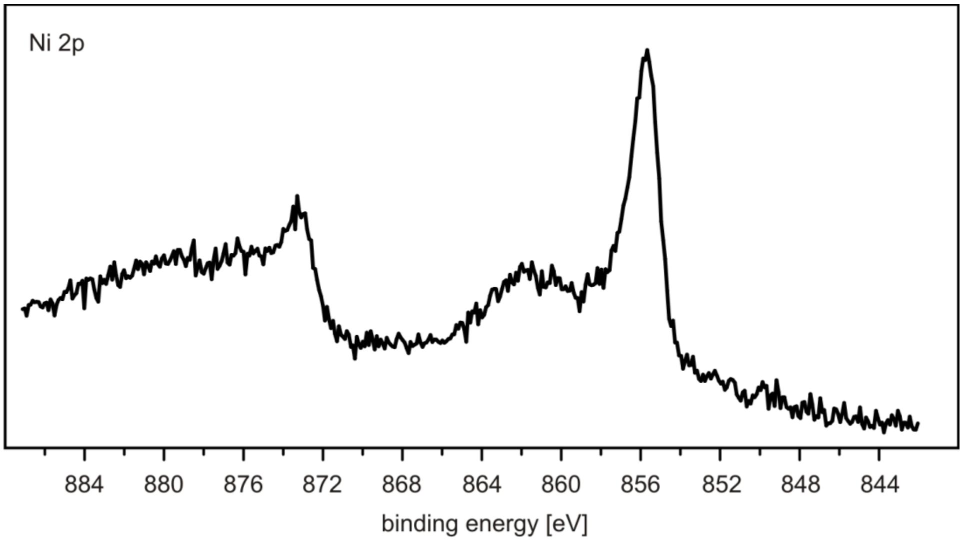

Fig. S35: Ni 2p core level spectrum of ***t*BuMC$_2$Ni**, with underlying Fluorine Auger signals.

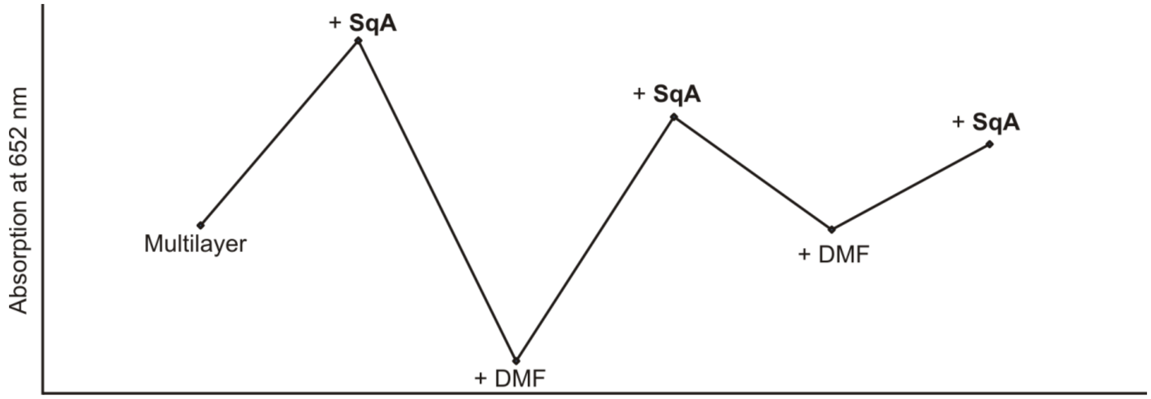

Fig. S36: Plot of absorption intensity at 652 nm after alternating deposition of **SqA** and removal through addition of DMF on a multilayer assembly with 9 **MC** and Fe(II).

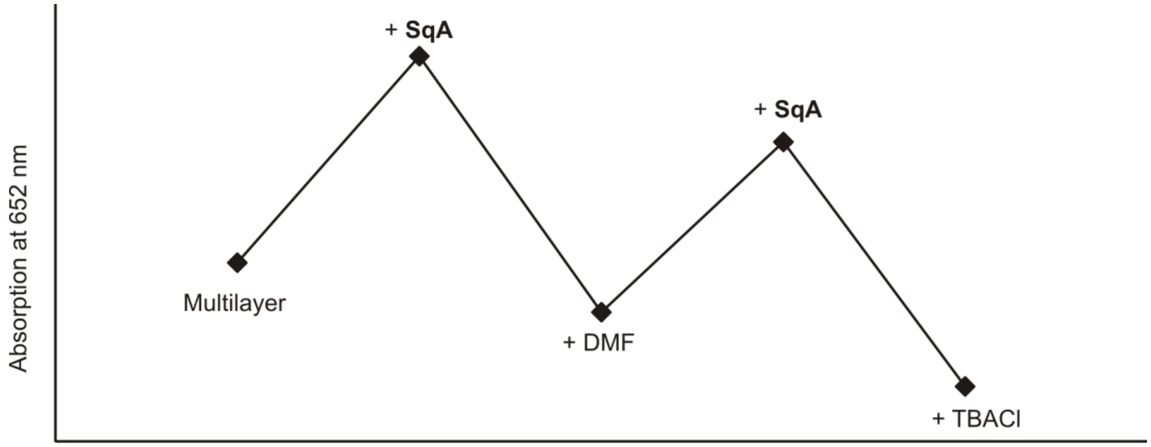

Fig. S37: Plot of absorption intensity at 652 nm after alternating deposition of **SqA** and removal through addition of DMF or *tert*-butylammonium chloride (TBACl) in DCM on a multilayer assembly with 9 **MC** and Ni(II).

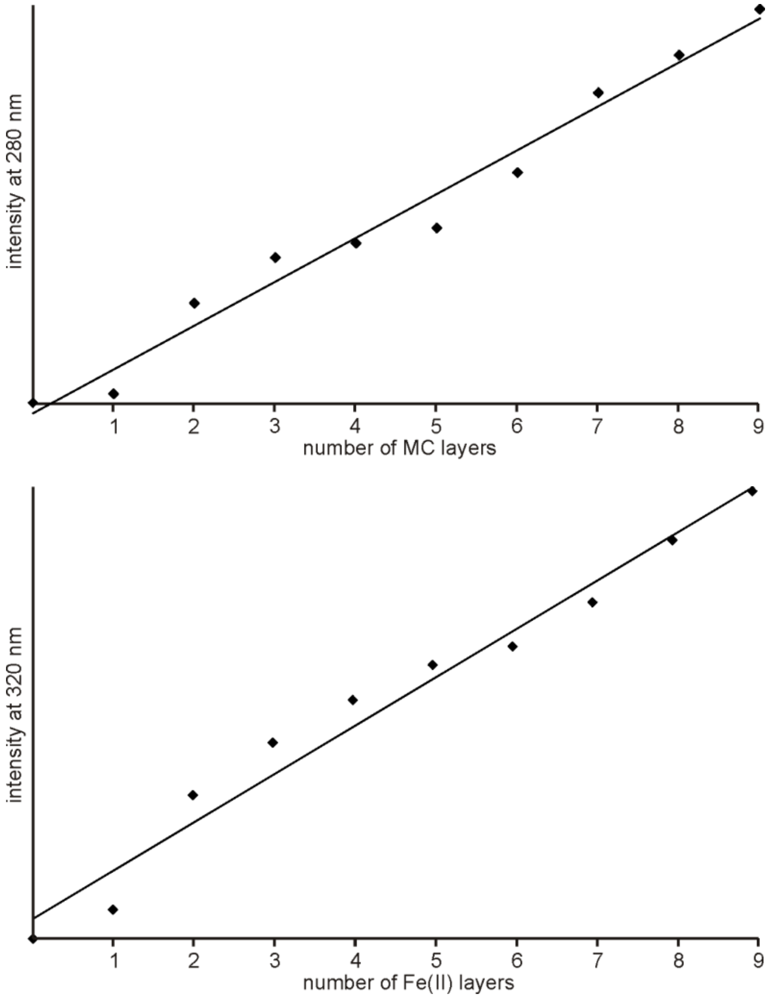

Fig. S38: Top: Plot of π→π* band absorption intensities of an additional **TDT**/**DT** (1/3)-(Fe-**MC**)$_x$ multilayer over the number of deposited macrocycles including a linear fit. Bottom: Plot of LC band absorption intensities of the same experiment over the number of deposited Fe(II) layers including a linear fit. This experiment is one of several repetitions of the multilayer construction experiment shown in the main text in **Fig.** 2.

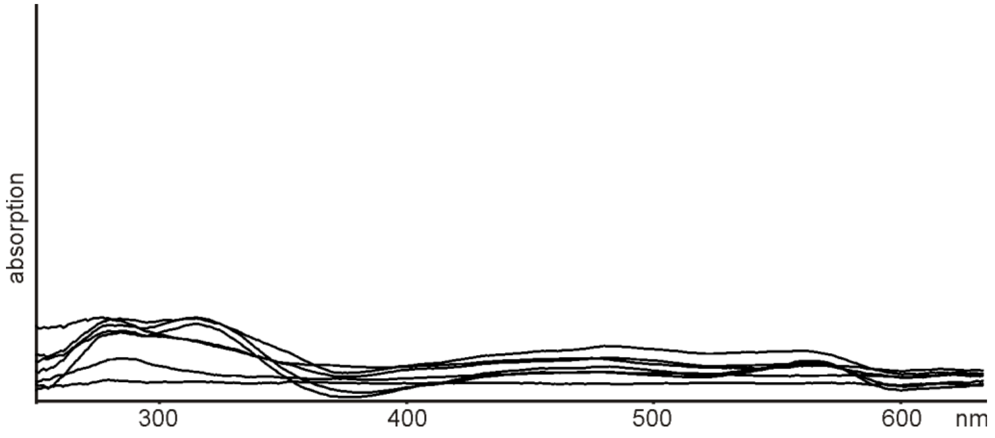

Fig. S39: Transmission-UV/Vis spectra of unsuccessful multilayer formation with **MC** and Fe(II) ions using a **TDT**/**DT** 1/20 template layer, recorded after each macrocycle deposition. No controlled growth is observed here.

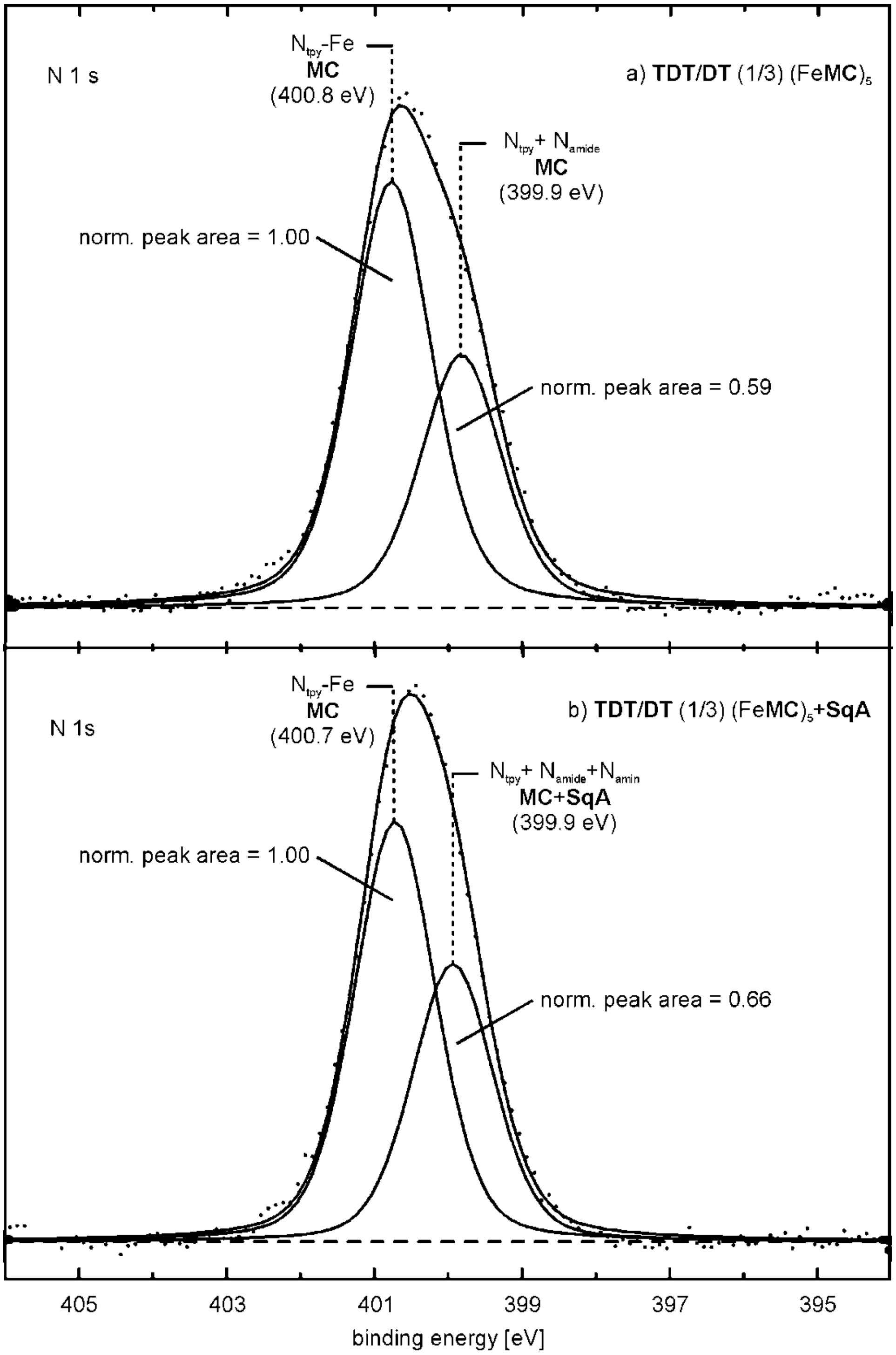

Fig. S40: XP N 1s core-level spectrum of a) **TDT**/**DT** 1/3-(Fe-**MC**)$_5$ and b) **TDT**/**DT** 1/3-(Fe-**MC**)$_5$ +**SqA** . Peaks in a) do exclusively include contributions from **MC** and to some extend nitrogen atoms of the templating SAM. Peaks in b) additionally contain **SqA** nitrogen atoms. The component at 400.8 eV can be assigned to complexed terpyridine whereas the component at 399.9 eV is assigned to non-complexed terpyridine, amide and amine nitrogen atoms. The normalized peak area ratio of the component peak at 399.6 eV is higher in b) due to the addition of **SqA** which contains two N atoms. The ratio of the overall normalized peak area ratios a)/b) is 1.044. Therefore, 0.044 **SqA** nitrogen atoms are added for each **MC** nitrogen. Taking into account that MC contains 10 nitrogen atoms while **SqA** incorporates 2 nitrogen atoms gives rise to an estimate of 1 **SqA** per 4 to 5 **MC** molecules.

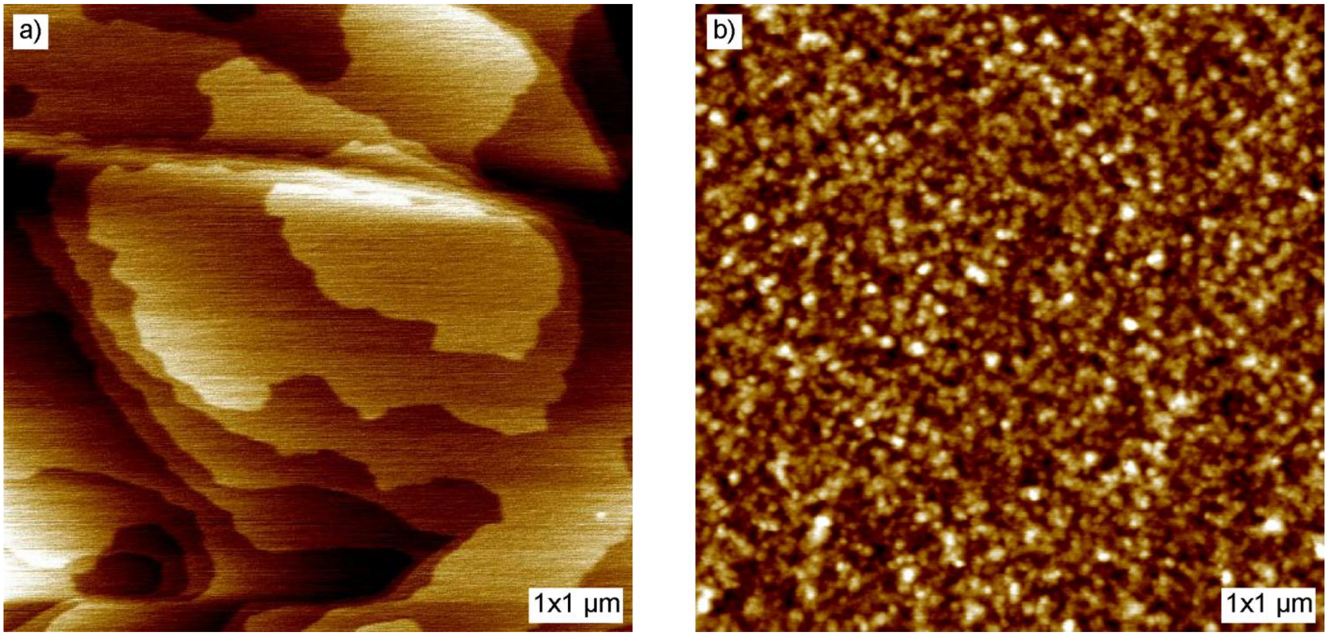

Fig. S41: AFM height images of a) a blank gold surface and b) a **TDT**/**DT** 1/3-(Fe-**MC**)$_5$ multilayer. A significant morphological change and a rather homogenous structure at the interface are observed after multilayer formation.

References

1 ISO15472:2010. (2010).

2 Merzlikin, S. V.; Tolkachev, N. N.; Strunskus, T.; Witte, G.; Glogowski, T.; Wöll, C.; Grünert, W. *Surf. Sci.* **2008**, *602*, 755-767.

3 Seah, M. P.; Dench, W. A. *Surf. Interface Anal.* **1979**, *1*, 2-11.

4 Seah, M. P.; Spencer, S. J. *Surf. Interface Anal.* **2011**, *43*, 744-751.

5 Tanuma, S.; Powell, C. J.; Penn, D. R. *Surf. Interface Anal.* **1993**, *20*, 77-89.

6 Brundle, C. R.; Hopster, H.; Swalen, J. D. *J. Chem. Phys.* **1979**, *70*, 5190-5196.

7 Laibinis, P. E.; Bain, C. D.; Whitesides, G. M. *J. Phys. Chem.* **1991**, *95*, 7017-7021.

8 Stöhr, J. *NEXAFS Spectroscopy*, Springer, Heidelberg 1992.

9 Batson, P. E. *Phys. Rev. Lett.* **1982**, *49*, 936-940.

10 Baytekin, B.; Zhu, S. S.; Brusilowskij, B.; Illigen, J.; Ranta, J.; Huuskonen, J.; Rissanen, K.; Kaufmann, L.; Schalley, C. A. *Chem. Eur. J.* **2008**, *14*, 10012-10028.

11 Dzyuba, E. V.; Baytekin, B.; Sattler, D.; Schalley, C. A. *Eur. J. Org. Chem.* **2012**, 1171-1178.

12 Gassensmith, J. J.; Barr, L.; Baumes, J. M.; Paek, A.; Nguyen, A.; Smith, B.D. *Org. Lett.* **2008**, *10*, 3343-3346.